

Search for CP violation and measurement of branching fractions and decay asymmetry parameters for $\Lambda_c^+ \rightarrow \Lambda h^+$ and $\Lambda_c^+ \rightarrow \Sigma^0 h^+$ ($h = K, \pi$)

(The Belle Collaboration)

We report a study of $\Lambda_c^+ \rightarrow \Lambda h^+$ and $\Lambda_c^+ \rightarrow \Sigma^0 h^+$ ($h = K, \pi$) decays based on a data sample of 980 fb^{-1} collected with the Belle detector at the KEKB energy-asymmetric e^+e^- collider. The first results of direct CP asymmetry in two-body singly Cabibbo-suppressed (SCS) decays of charmed baryons are measured, $A_{CP}^{\text{dir}}(\Lambda_c^+ \rightarrow \Lambda K^+) = +0.021 \pm 0.026 \pm 0.001$ and $A_{CP}^{\text{dir}}(\Lambda_c^+ \rightarrow \Sigma^0 K^+) = +0.025 \pm 0.054 \pm 0.004$. We also make the most precise measurement of the decay asymmetry parameters (α) for the four modes of interest and search for CP violation via the α -induced CP asymmetry (A_{CP}^α). We measure $A_{CP}^\alpha(\Lambda_c^+ \rightarrow \Lambda K^+) = -0.023 \pm 0.086 \pm 0.071$ and $A_{CP}^\alpha(\Lambda_c^+ \rightarrow \Sigma^0 K^+) = +0.08 \pm 0.35 \pm 0.14$, which are the first A_{CP}^α results for SCS decays of charmed baryons. We search for Λ -hyperon CP violation in $\Lambda_c^+ \rightarrow (\Lambda, \Sigma^0)\pi^+$ and find $A_{CP}^\alpha(\Lambda \rightarrow p\pi^-) = +0.013 \pm 0.007 \pm 0.011$. This is the first time that hyperon CP violation has been measured via Cabibbo-favored charm decays. No evidence of baryon CP violation is found. We also obtain the most precise branching fractions for two SCS Λ_c^+ decays, $\mathcal{B}(\Lambda_c^+ \rightarrow \Lambda K^+) = (6.57 \pm 0.17 \pm 0.11 \pm 0.35) \times 10^{-4}$ and $\mathcal{B}(\Lambda_c^+ \rightarrow \Sigma^0 K^+) = (3.58 \pm 0.19 \pm 0.06 \pm 0.19) \times 10^{-4}$. The first uncertainties are statistical and the second systematic, while the third uncertainties come from the uncertainties on the world average branching fractions of $\Lambda_c^+ \rightarrow (\Lambda, \Sigma^0)\pi^+$.

Keywords: CP violation, charmed baryon, singly Cabibbo-suppressed decay, branching fraction, decay asymmetry parameter, CP asymmetry

I. INTRODUCTION

Charge-parity (CP) violation is one of the conditions necessary to explain the matter-antimatter asymmetry of the universe [1]. The single complex phase in the Cabibbo-Kobayashi-Maskawa matrix provides the only source of CP violation (CPV) in the standard model (SM), but it is not large enough to explain the observed matter-antimatter asymmetry. Baryogenesis, the process by which the baryon-antibaryon asymmetry of the universe developed, is directly related to baryon CPV [2, 3]. To date, CPV has been observed in the open-flavored meson sector, but not yet established in the baryon sector. Since CPV in charm decays is predicted in the SM to be at the level of 10^{-3} or smaller [4–8], an observation of CPV in charm decays much greater than 10^{-3} could indicate new physics beyond the SM [9–12].

Singly Cabibbo-suppressed (SCS) decays of charm hadrons provide an ideal laboratory for studying CPV as they are a unique window on the physics of decay-rate dynamics in the charm sector [8, 12]. The only observation of CPV in the charm sector was made by the LHCb collaboration in SCS charmed meson decays, $D^0 \rightarrow h^+ h^-$ ($h = K, \pi$ throughout this paper) [13]. Measurements of the direct CP asymmetry (A_{CP}^{dir}), induced by the partial widths, in SCS charmed baryon decays are experimentally more challenging than in charmed meson decays and relatively unexplored. Searches for direct CPV in SCS charmed baryon decays were made in $\Lambda_c^+ \rightarrow p h^+ h^-$ [14] and $\Xi_c^+ \rightarrow p K^- \pi^+$ [15]. No direct CPV searches in two-body SCS decays of charmed baryons have been made.

In addition to A_{CP}^{dir} , the α -induced CP asymmetry (A_{CP}^α) is an essential observable to search for CPV in baryon decays. Here α is the decay asymmetry parameter introduced to study the parity-violating

and parity-conserving amplitudes in weak hyperon decays [16]. In a weak decay of Λ_c^+ into a spin 1/2 baryon with positive parity and a pseudoscalar meson, $\alpha \equiv 2 \cdot \text{Re}(S^*P)/(|S|^2 + |P|^2)$, where S and P denote the parity-violating S -wave and parity-conserving P -wave amplitudes, respectively. Since α is CP -odd, the α -induced CP asymmetry for Λ_c^+ decays is defined as $A_{CP}^\alpha \equiv (\alpha_{\Lambda_c^+} + \alpha_{\bar{\Lambda}_c^-})/(\alpha_{\Lambda_c^+} - \alpha_{\bar{\Lambda}_c^-})$. In the case that A_{CP}^{dir} is zero, A_{CP}^α is given by the CPV in $\text{Re}(S^*P)$. Therefore, A_{CP}^α provides an observable complementary to A_{CP}^{dir} . To date, there is only one A_{CP}^α measurement for hadronic Λ_c^+ decays, $A_{CP}^\alpha(\Lambda_c^+ \rightarrow \Lambda \pi^+) = -0.07 \pm 0.22$ [17]. Using the precisely measured α_{\mp} in $\Lambda \rightarrow p\pi^-$ decays [18] and the high-statistics Λ_c^+ sample at Belle, we obtain the $\alpha_{\Lambda_c^+}$ and $\alpha_{\bar{\Lambda}_c^-}$ values in $\Lambda_c^+ \rightarrow (\Lambda, \Sigma^0)h^+$ decays, described in detail in Sec. III, make the first measurements of A_{CP}^α in $\Lambda_c^+ \rightarrow \Lambda K^+$ and $\Lambda_c^+ \rightarrow \Sigma^0 h^+$ decays, and measure A_{CP}^α with improved precision in $\Lambda_c^+ \rightarrow \Lambda \pi^+$.

The Λ -hyperon CP asymmetry $A_{CP}^\alpha(\Lambda \rightarrow p\pi^-)$ can be extracted from the total α -induced CP asymmetry ($A_{CP}^\alpha(\text{total}) \equiv (\alpha_{\Lambda_c^+} \alpha_- - \alpha_{\bar{\Lambda}_c^-} \alpha_+)/(\alpha_{\Lambda_c^+} \alpha_- + \alpha_{\bar{\Lambda}_c^-} \alpha_+)$) for Cabibbo-favored (CF) decays $\Lambda_c^+ \rightarrow (\Lambda, \Sigma^0)\pi^+$ with $\alpha_{\Lambda_c^+} = -\alpha_{\bar{\Lambda}_c^-}$ since no CP asymmetry is expected in the SM. CPV in hyperon decays is predicted to be at the level of $\mathcal{O}(10^{-4})$ or smaller in the SM [19–22] and can be enhanced to reach the level of 10^{-3} in some new physics models [22–26]. This analysis is a novel and complementary method, proposed in Ref. [27], for Λ -hyperon CPV searches.

Since the Λ_c^+ was discovered, many efforts have been made to predict the branching fractions (BF) and α parameters of its hadronic decays using phenomenological models such as current algebra [28], pole model [29, 30] and $\text{SU}(3)_F$ symmetry [31–35]. These predictions are

nontrivial due to non-perturbative strong dynamics, which complicate the calculation of non-factorizable contributions [36, 37]. Experimentally, studies of charmed baryon decays are more challenging than those of charmed mesons due to lower production rates. The current world averages $\mathcal{B}(\Lambda_c^+ \rightarrow \Lambda K^+) = (6.1 \pm 1.2) \times 10^{-4}$ and $\mathcal{B}(\Lambda_c^+ \rightarrow \Sigma^0 \pi^+) = (5.2 \pm 0.8) \times 10^{-4}$ [38], rely on measurements with partial datasets from Belle and BaBar [39, 40]. We perform a measurement based on a dataset thirty times larger than previously used, superseding the result in Ref. [39].

In this paper, we report A_{CP}^{dir} and BF measurements for the SCS decays $\Lambda_c^+ \rightarrow \Lambda K^+$ and $\Lambda_c^+ \rightarrow \Sigma^0 K^+$, using the CF decays $\Lambda_c^+ \rightarrow \Lambda \pi^+$ and $\Lambda_c^+ \rightarrow \Sigma^0 \pi^+$ as reference modes. Inclusion of charge conjugate states is implicit, unless otherwise stated. We also measure α and A_{CP}^α in these four decays and search for Λ -hyperon CPV in the CF Λ_c^+ decays.

II. DETECTOR AND DATA SET

This analysis is based on the full data set recorded by the Belle detector [41, 42] operating at the KEKB [43, 44] asymmetric-energy e^+e^- collider. This data sample corresponds to a total integrated luminosity of 980 fb^{-1} collected at or near the $\Upsilon(nS)$ ($n=1, 2, 3, 4, 5$) resonances. The Belle detector is a large-solid-angle magnetic spectrometer consisting of a silicon vertex detector (SVD), a central drift chamber (CDC), an array of aerogel threshold Cherenkov counters (ACC), a barrel-like arrangement of time-of-flight scintillation counters (TOF), and an electromagnetic calorimeter (ECL) consisting of CsI(Tl) crystals. These components are all located inside a superconducting solenoid coil that provides a 1.5 T magnetic field. The iron flux-return of the magnet is instrumented to detect K_L^0 mesons and to identify muons (KLM). The detector is described in detail elsewhere [41, 42].

Monte Carlo (MC) simulated events are generated with EVTGEN [45] and PYTHIA [46], and are subsequently processed through a full detector simulation based on GEANT3 [47]. Final-state radiation from charged particles is included at event generation using PHOTOS [48]. Signal Λ_c^+ baryons are produced via the inclusive process $e^+e^- \rightarrow c\bar{c} \rightarrow \Lambda_c^+ + \text{anything}$ and $\Lambda_c^+ \rightarrow \Lambda h^+$, $\Sigma^0 h^+$ decays, where $\Sigma^0 \rightarrow \Lambda \gamma$ and $\Lambda \rightarrow p \pi^-$.

III. MEASUREMENT METHODS

The direct CP asymmetry, taking Λ_c^+ decays as an example, is defined as

$$A_{CP}^{\text{dir}} = \frac{\Gamma(\Lambda_c^+ \rightarrow f) - \Gamma(\bar{\Lambda}_c^- \rightarrow \bar{f})}{\Gamma(\Lambda_c^+ \rightarrow f) + \Gamma(\bar{\Lambda}_c^- \rightarrow \bar{f})}, \quad (1)$$

where $\Gamma(\Lambda_c^+ \rightarrow f)$ and $\Gamma(\bar{\Lambda}_c^- \rightarrow \bar{f})$ are the partial decay widths for the final state f and its CP -conjugate state \bar{f} . The raw asymmetry in the decays of $\Lambda_c^+ \rightarrow f$ and $\bar{\Lambda}_c^- \rightarrow \bar{f}$ is defined with signal yields N as follows:

$$A_{\text{raw}} = \frac{N(\Lambda_c^+ \rightarrow f) - N(\bar{\Lambda}_c^- \rightarrow \bar{f})}{N(\Lambda_c^+ \rightarrow f) + N(\bar{\Lambda}_c^- \rightarrow \bar{f})}. \quad (2)$$

Several sources contribute to the raw asymmetry, which for $\Lambda_c^+ \rightarrow \Lambda K^+$ is given by

$$A_{\text{raw}} = A_{CP}^{\Lambda_c^+ \rightarrow \Lambda K^+} + A_{CP}^{\Lambda \rightarrow p \pi^-} + A_\varepsilon^\Lambda + A_\varepsilon^{K^+} + A_{\text{FB}}^{\Lambda_c^+}, \quad (3)$$

where all terms are small (at the level of 10^{-2} or smaller). Here $A_{CP}^{\Lambda_c^+ \rightarrow \Lambda K^+}$ ($A_{CP}^{\Lambda \rightarrow p \pi^-}$) is the direct CP asymmetry associated with the Λ_c^+ (Λ) decay, A_ε^Λ ($A_\varepsilon^{K^+}$) is the detection asymmetry resulting from differences in the reconstruction efficiency between Λ (K^+) and its anti-particle $\bar{\Lambda}$ (K^-), and $A_{\text{FB}}^{\Lambda_c^+}$ arises from the forward-backward asymmetry (FBA) of Λ_c^+ production due to γ - Z^0 interference and higher-order QED effects in $e^+e^- \rightarrow c\bar{c}$ collisions [49, 50]. The FBA is an odd function in $\cos \theta^*$, where θ^* is the Λ_c^+ production polar angle in the e^+e^- center-of-mass frame, but due to asymmetric acceptance, small residual asymmetry remains after integrating over $\cos \theta^*$.

We weight Λ_c^\pm candidates with factors $1 \mp A_\varepsilon^{h^\pm}$ to remove the K^+ or π^+ detection asymmetry from the raw asymmetry in $\Lambda_c^+ \rightarrow (\Lambda, \Sigma^0)K^+$ or $\Lambda_c^+ \rightarrow (\Lambda, \Sigma^0)\pi^+$. We use $A_{\text{raw}}^{\text{corr}}$ to indicate this corrected raw asymmetry. Here $A_\varepsilon^{h^\pm}$ depends on the cosine of the polar angle and transverse momentum of the h^\pm tracks in the laboratory frame and was determined at Belle using $D^0 \rightarrow K^- \pi^+$ and $D_s^+ \rightarrow \phi \pi^+$ events for $A_\varepsilon^{K^+}$ [51] and $D^+ \rightarrow K^- \pi^+ \pi^+$ and $D^0 \rightarrow K^- \pi^+ \pi^0$ events for $A_\varepsilon^{\pi^+}$ [52]. The signal modes and corresponding reference modes have nearly the same Λ kinematic distributions, including the Λ decay length, the polar angle with respect to the direction opposite the positron beam and the momentum of the proton and pion in the laboratory reference frame. Asymmetries common between the signal and reference modes therefore cancel.

The difference of the corrected raw asymmetries is

$$\begin{aligned} & A_{\text{raw}}^{\text{corr}}(\Lambda_c^+ \rightarrow \Lambda K^+) - A_{\text{raw}}^{\text{corr}}(\Lambda_c^+ \rightarrow \Lambda \pi^+) \\ &= A_{CP}^{\text{dir}}(\Lambda_c^+ \rightarrow \Lambda K^+) - A_{CP}^{\text{dir}}(\Lambda_c^+ \rightarrow \Lambda \pi^+). \end{aligned} \quad (4)$$

The direct CP asymmetry for $\Lambda_c^+ \rightarrow \Lambda \pi^+$, a CF process with an amplitude that has only one weak phase, can be set to be zero. Thus, the measured asymmetry difference in Eq. (4) is equal to A_{CP}^{dir} for $\Lambda_c^+ \rightarrow \Lambda K^+$.

The BF's of signal modes are measured relative to those of the reference modes using

$$\frac{\mathcal{B}_{\text{sig}}}{\mathcal{B}_{\text{ref}}} = \frac{N_{\text{sig}}/\varepsilon_{\text{sig}}}{N_{\text{ref}}/\varepsilon_{\text{ref}}}, \quad (5)$$

where N_{sig} is the extracted signal yield and ε is the reconstruction efficiency. The world average values $\mathcal{B}(\Lambda_c^+ \rightarrow \Lambda\pi^+) = (1.30 \pm 0.07)\%$ and $\mathcal{B}(\Lambda_c^+ \rightarrow \Sigma^0\pi^+) = (1.29 \pm 0.07)\%$ [38] are used for the reference modes. The common systematic uncertainties between the signal modes and reference modes, such as the inclusive Λ_c^+ yield produced from $e^+e^- \rightarrow c\bar{c}$ and the mass resolution of the Λ and Σ^0 , cancel in the ratio.

For $\Lambda_c^+ \rightarrow \Lambda h^+$ decays, the differential decay rate depends on α parameters and one helicity angle as

$$\frac{dN}{d\cos\theta_A} \propto 1 + \alpha_{\Lambda_c^+} \alpha_- \cos\theta_A, \quad (6)$$

where $\alpha_{\Lambda_c^+}$ is the decay asymmetry parameter of $\Lambda_c^+ \rightarrow \Lambda h^+$, and θ_A is the angle between the proton momentum and the direction opposite the Λ_c^+ momentum in the Λ rest frame, as illustrated in the supplemental materials. For $\Lambda_c^+ \rightarrow \Sigma^0 h^+$ decays, considering $\alpha(\Sigma^0 \rightarrow \gamma\Lambda)$ is zero due to parity conservation for an electromagnetic decay, the differential decay rate is given by

$$\frac{dN}{d\cos\theta_{\Sigma^0} d\cos\theta_A} \propto 1 - \alpha_{\Lambda_c^+} \alpha_- \cos\theta_{\Sigma^0} \cos\theta_A, \quad (7)$$

where θ_A (θ_{Σ^0}) is the angle between the proton (Λ) momentum and the direction opposite the Σ^0 (Λ_c^+) momentum in the Λ (Σ^0) rest frame, as illustrated in the supplemental materials.

IV. EVENT SELECTION AND OPTIMIZATION

The h^+ candidates from Λ_c^+ decays are selected as follows. Charged tracks satisfying $\mathcal{R}(K|\pi) = \mathcal{L}_K/(\mathcal{L}_K + \mathcal{L}_\pi) > 0.7$ are identified as kaons, while those satisfying $\mathcal{R}(K|\pi) < 0.7$ are identified as pions. Here \mathcal{L}_i ($i = \pi, K, p$) is the particle identification (PID) likelihood for a given particle hypothesis, which is calculated from the photon yield in the ACC, energy-loss measurements in the CDC, and time-of-flight information from the TOF [53]. The highly proton-like tracks with $\mathcal{R}(p|K) > 0.8$ and $\mathcal{R}(p|\pi) > 0.8$ are rejected as h^+ candidates for signal modes and reference modes, respectively. To suppress the background from Λ_c^+ semileptonic decays, tracks that are highly electron-like ($\mathcal{L}_e/(\mathcal{L}_e + \mathcal{L}_{\text{non-}e}) > 0.95$) or muon-like ($\mathcal{L}_\mu/(\mathcal{L}_\mu + \mathcal{L}_\pi + \mathcal{L}_K) > 0.95$) are rejected. The electron and muon likelihoods depend primarily on the information from the ECL and KLM, respectively [54, 55]. The signal efficiency after applying PID requirements is 83% for signal modes and 96% for reference modes. About 44% and 9% of total backgrounds are rejected for signal modes and reference modes, respectively. We require the h^+ candidates to have at least two hits in the SVD to improve their impact parameter resolution with respect to the interaction point.

The Λ candidates are reconstructed from one p and one π candidate, which a fit requires to originate from

a common vertex. We require $|M_\Lambda - m_\Lambda| < 3 \text{ MeV}/c^2$, corresponding to approximately 2.5 standard deviations of the M_Λ resolution. Proton candidates are required to have $\mathcal{R}(p|K) > 0.2$. To suppress the non- Λ background, we calculate the significance of the Λ decay length (L/σ_L), where L is the projection of the Λ displacement vector, relative to the production vertex, onto its momentum direction. The corresponding uncertainty σ_L is calculated by propagating uncertainties in the vertices and the Λ momentum, including their correlations. We require $L/\sigma_L > 4$ to suppress the non- Λ background. The signal efficiency loss due to this requirement is 5% for all decay modes and the background rejection rate is 22% for $\Lambda_c^+ \rightarrow \Lambda K^+$, 35% for $\Lambda_c^+ \rightarrow \Lambda\pi^+$, 19% for $\Lambda_c^+ \rightarrow \Sigma^0 K^+$ and 23% for $\Lambda_c^+ \rightarrow \Sigma^0\pi^+$.

Photon candidates are identified as energy clusters in the ECL that are not associated with any charged track. The ratio of the energy deposited in the 3×3 array of crystals centered on the crystal with the highest energy to the energy deposited in the corresponding 5×5 array is required to be greater than 0.85. Candidate $\Sigma^0 \rightarrow \Lambda\gamma$ decays are formed by combining the Λ candidate with a photon candidate that has an ECL cluster energy above 0.1 GeV. The Σ^0 candidate is required to have $|M(\Sigma^0) - m_{\Sigma^0}| < 6 \text{ MeV}/c^2$, corresponding to 1.5 standard deviations of the $M(\Sigma^0)$ resolution.

Candidate $\Lambda_c^+ \rightarrow \Lambda h^+$ and $\Lambda_c^+ \rightarrow \Sigma^0 h^+$ decays are reconstructed by combining Λ or Σ^0 candidate with a h^+ candidate. A fit constrains the Λ and h^+ candidates to originate from a common vertex and the χ^2 of the fit is required to be less than 9. To suppress combinatorial backgrounds, the normalized momentum $x_p = p^*c/\sqrt{s/4 - M^2(\Lambda_c^+) \cdot c^4}$ is required to be greater than 0.5, where p^* is the Λ_c^+ momentum in e^+e^- center-of-mass frame and \sqrt{s} is the center-of-mass energy.

We improve the invariant mass resolution by calculating the corrected mass difference wherever the final state includes a hyperon. Taking $\Lambda_c^+ \rightarrow \Lambda h^+$ as an example, the corrected mass is $M(\Lambda_c^+) = M_{\Lambda_c^+} - M_\Lambda + m_\Lambda$ where M_X is the invariant mass of reconstructed particle X and m_X represents its nominal mass [38]. The event selection criteria above are optimized with a figure-of-merit (FOM), which is defined as $S/\sqrt{S+B}$ where S and B are the expected signal and background yields in the signal region. The signal region is defined as $|M(\Lambda_c^+) - m_{\Lambda_c^+}| < 15 \text{ MeV}/c^2$, corresponding to 2.5 standard deviations in the $M(\Lambda_c^+)$ resolution.

After applying the optimized requirements, the Λ_c^+ candidate multiplicity is greater than one for 1%, 7%, 7%, and 11% of events for $\Lambda_c^+ \rightarrow \Lambda K^+$, $\Lambda\pi^+$, $\Sigma^0 K^+$, and $\Sigma^0\pi^+$, respectively. For modes including a Σ^0 , the multiplicity is predominantly from multiple photons. We perform a best candidate selection (BCS) for events with multiple candidates by retaining candidates with the smallest sum of χ^2 from the vertex fits of the Λ and

Λ_c^+ candidates for $\Lambda_c^+ \rightarrow \Lambda h^+$ modes. For $\Lambda_c^+ \rightarrow \Sigma^0 h^+$ modes, an additional term given by $(M(\Sigma^0) - m_{\Sigma^0})^2 / \sigma_M^2$ where $\sigma_M = 4 \text{ MeV}/c^2$ is the Σ^0 mass resolution, is added. The BCS has a signal efficiency of 60% for events with multiple candidates and does not introduce any peaking backgrounds.

V. DIRECT CP ASYMMETRY

The signal probability density function (PDF) is described by a sum of three or four asymmetric Gaussian functions for SCS or CF modes, respectively. These Gaussian functions share a common mean parameter but have different width parameters. For modes that include a Σ^0 , an additional component denoted broken- Σ^0 signal, which is the signal decay but with the γ in $\Sigma^0 \rightarrow \Lambda\gamma$ replaced by a random photon in the event, is added into the signal and its shape and ratio to the total signal are fixed according to the results of a fit to the MC sample. Such ratio is 16.2% in $\Lambda_c^+ \rightarrow \Sigma^0 K^+$ and 15.5% in $\Lambda_c^+ \rightarrow \Sigma^0 \pi^+$ and the shape is shown in the supplemental materials. The signal parameters are fixed to the fitted results of truth-matched signal, but with a common shift (δ_μ) for the mean parameter and a common scaling factor (k_σ) for all width parameters to account for discrepancies between the experimental data and simulated samples.

The background PDF is constructed from a sum of empirical shapes based on truth-matched background events in simulation and a second-order polynomial function for $\Lambda_c^+ \rightarrow \Lambda K^+$ or a third-order polynomial for the other modes. For $\Lambda_c^+ \rightarrow \Lambda K^+$, the empirical backgrounds include $\Lambda_c^+ \rightarrow \Lambda \pi^+$ decays with the π^+ misidentified as a K^+ , a feed-down background from $\Lambda_c^+ \rightarrow \Sigma^0 K^+$ with a missing γ , and a wide enhancement of $\Lambda_c^+ \rightarrow \Sigma^0 \pi^+$ with a misidentified π^+ and a missing γ . For $\Lambda_c^+ \rightarrow \Lambda \pi^+$, the empirical backgrounds include a feed-down background from $\Lambda_c^+ \rightarrow \Sigma^0 \pi^+$, and a feed-down Ξ_c background from $\Xi_c^{0,+} \rightarrow \Xi^{-,0} \pi^+$ where $\Xi^{-,0} \rightarrow \Lambda \pi^{-,0}$ with one missing pion. For $\Lambda_c^+ \rightarrow \Sigma^0 K^+$, the empirical backgrounds include a background from $\Lambda_c^+ \rightarrow \Sigma^0 \pi^+$ with a misidentified π^+ and a feed-down background from $\Lambda_c^+ \rightarrow \Xi^0 K^+$ where $\Xi^0 \rightarrow \Lambda \pi^0$, $\pi^0 \rightarrow \gamma\gamma$ with one missing photon. For $\Lambda_c^+ \rightarrow \Sigma^0 \pi^+$, the empirical backgrounds include a reflection background from $\Lambda_c^+ \rightarrow \Lambda \pi^+$ where Λ is combined with a random γ to form fake Σ^0 candidate. The yields of each component and the parameters of the polynomial functions are floated to account for discrepancies between the experimental data and simulated samples.

We perform an unbinned extended maximum likelihood fit on the $M(\Lambda_c^\pm)$ distributions of the weighted Λ_c^+ and $\bar{\Lambda}_c^-$ samples simultaneously to measure the corrected raw asymmetries. In the fit, the mass resolution of Λ_c^+ and $\bar{\Lambda}_c^-$ are allowed to differ. The fractions of broken- Σ^0 signal are fixed to those for the Λ_c^+ and $\bar{\Lambda}_c^-$ MC samples, separately. The fit projections are shown in Fig. 1 for

$\Lambda_c^+ \rightarrow \Lambda h^+$ and in Fig. 2 for $\Lambda_c^+ \rightarrow \Sigma^0 h^+$, along with the distribution of pull values, defined as $(N_{\text{data}} - N_{\text{fit}}) / \sigma_{\text{data}}$ where σ_{data} is the uncertainty on N_{data} . The fitted $A_{\text{raw}}^{\text{corr}}$ values with statistical uncertainties)¹ are

$$A_{\text{raw}}^{\text{corr}}(\Lambda_c^+ \rightarrow \Lambda K^+) = (+3.66 \pm 2.59)\%, \quad (8)$$

$$A_{\text{raw}}^{\text{corr}}(\Lambda_c^+ \rightarrow \Lambda \pi^+) = (+1.55 \pm 0.30)\%, \quad (9)$$

$$A_{\text{raw}}^{\text{corr}}(\Lambda_c^+ \rightarrow \Sigma^0 K^+) = (+7.71 \pm 5.35)\%, \quad (10)$$

$$A_{\text{raw}}^{\text{corr}}(\Lambda_c^+ \rightarrow \Sigma^0 \pi^+) = (+5.23 \pm 0.40)\%. \quad (11)$$

Using Eq. (4), we measure the CP asymmetries:

$$A_{CP}^{\text{dir}}(\Lambda_c^+ \rightarrow \Lambda K^+) = (+2.1 \pm 2.6 \pm 0.1)\%, \quad (12)$$

$$A_{CP}^{\text{dir}}(\Lambda_c^+ \rightarrow \Sigma^0 K^+) = (+2.5 \pm 5.4 \pm 0.4)\%, \quad (13)$$

where the first uncertainties are statistical and the second are systematic, which are discussed in detail below. No evidence of charm CP violation is found. This is the first direct CP asymmetry measurement for SCS two-body decays of charmed baryons.

For the measurements of A_{CP}^{dir} described here, as well as the BF, α , and A_{CP}^α measurements described later, we validated our fitting procedure using simulated samples, along with “toy” MC samples in which events were generated by sampling from the PDFs that were fit to the data. In all cases, the fit results were consistent with the input values used to generate events and with correct fit uncertainties.

VI. BRANCHING FRACTION

To measure the BF, we perform a fit to the $M(\Lambda_c^\pm)$ distribution for the combined Λ_c^+ and $\bar{\Lambda}_c^-$ sample. The fitted signal yields are listed in Table I, along with the reconstruction efficiency ratio for the SCS modes relative to the CF modes. The efficiency is determined based on signal MC events, which are produced with a special angular distribution using our measured α values. An event-by-event correction (typically 0.3% and 2.8%) is applied to account for discrepancies in the K^+ and π^+ PID efficiencies between data and simulation. These correction factors depend on the momentum and polar angle of tracks and are determined using a sample of $D^{*+} \rightarrow [D^0 \rightarrow K^- \pi^+] \pi^+$ decays. Additional details are given in the supplemental materials.

Using the fitted yields and efficiency ratios, we calculate the BF ratios according to Eq. (5) as

$$\frac{\mathcal{B}(\Lambda_c^+ \rightarrow \Lambda K^+)}{\mathcal{B}(\Lambda_c^+ \rightarrow \Lambda \pi^+)} = (5.05 \pm 0.13 \pm 0.09)\%, \quad (14)$$

¹ The difference in $A_{\text{raw}}^{\text{corr}}$ between the two CF modes is mainly due to the efficiency asymmetry of $\Sigma^0 \rightarrow \Lambda\gamma$ reconstruction (due to the extra fake photons from anti-proton annihilation in the ECL) according to a MC study, but this asymmetry cancels in the A_{CP}^{dir} measurement.

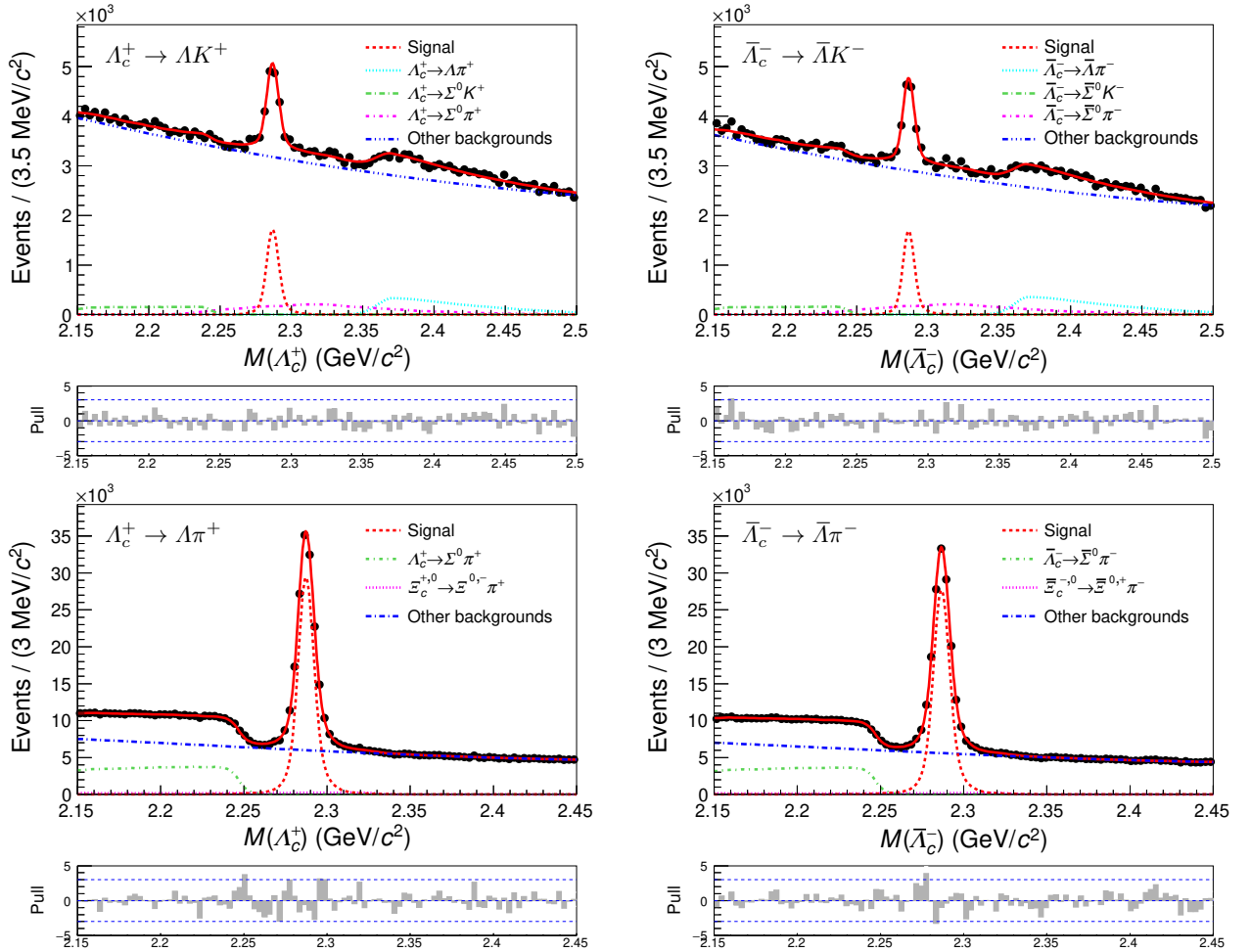


FIG. 1. The simultaneous fit to Λ_c^+ (left) and $\bar{\Lambda}_c^-$ (right) samples from real data for $\Lambda_c^+ \rightarrow \Lambda K^+$ (top) and $\Lambda_c^+ \rightarrow \Lambda \pi^+$ (bottom). The red curve is the total fitting result. The dashed lines show the components of signal and backgrounds (see text).

TABLE I. The fitted yield (N_{sig}), efficiency (ε) ratio, and ratio of branching fractions (\mathcal{B}) for signal modes $\Lambda_c^+ \rightarrow (\Lambda, \Sigma^0)K^+$ relative to reference modes $\Lambda_c^+ \rightarrow (\Lambda, \Sigma^0)\pi^+$, compared with the world average values (W.A.) [38].

Channel	N_{sig}	$\varepsilon_{\text{sig}}/\varepsilon_{\text{ref}}$	$\mathcal{B}_{\text{sig}}/\mathcal{B}_{\text{ref}}$ (%)	W.A.(%)
$\Lambda_c^+ \rightarrow \Lambda K^+$	11175 ± 296	0.836	$5.05 \pm 0.13 \pm 0.09$	4.7 ± 0.9
$\Lambda_c^+ \rightarrow \Lambda \pi^+$	264470 ± 787			
$\Lambda_c^+ \rightarrow \Sigma^0 K^+$	2436 ± 132	0.835	$2.78 \pm 0.15 \pm 0.05$	4.0 ± 0.6
$\Lambda_c^+ \rightarrow \Sigma^0 \pi^+$	105018 ± 475			

$$\frac{\mathcal{B}(\Lambda_c^+ \rightarrow \Sigma^0 K^+)}{\mathcal{B}(\Lambda_c^+ \rightarrow \Sigma^0 \pi^+)} = (2.78 \pm 0.15 \pm 0.05)\%, \quad (15)$$

where the first uncertainties are statistical and the second are systematic. Systematic uncertainties are described in detail in Sec. IX. These results are consistent with the recent results from BESIII, $\frac{\mathcal{B}(\Lambda_c^+ \rightarrow \Lambda K^+)}{\mathcal{B}(\Lambda_c^+ \rightarrow \Lambda \pi^+)} = (4.78 \pm 0.39)\%$ [56] within 0.6σ and $\frac{\mathcal{B}(\Lambda_c^+ \rightarrow \Sigma^0 K^+)}{\mathcal{B}(\Lambda_c^+ \rightarrow \Sigma^0 \pi^+)} = (3.61 \pm 0.73)\%$ [57] within 1.1σ , but with precision improved by threefold and fivefold, respectively.

Multiplying the BF results in Eqs.(14,15) by the world average values for the BF of the appropriate reference mode, $\mathcal{B}(\Lambda_c^+ \rightarrow \Lambda \pi^+) = (1.30 \pm 0.07)\%$ and $\mathcal{B}(\Lambda_c^+ \rightarrow \Sigma^0 \pi^+) = (1.29 \pm 0.07)\%$ [38], we measure the absolute branching fraction for the SCS decays,

$$\mathcal{B}(\Lambda_c^+ \rightarrow \Lambda K^+) = (6.57 \pm 0.17 \pm 0.11 \pm 0.35) \times 10^{-4}, \quad (16)$$

$$\mathcal{B}(\Lambda_c^+ \rightarrow \Sigma^0 K^+) = (3.58 \pm 0.19 \pm 0.06 \pm 0.19) \times 10^{-4}, \quad (17)$$

where the first uncertainties are statistical, the second are systematic, and the third are from the uncertainties on the BFs for the reference modes. These results are consistent with current world average values [38], $\mathcal{B}(\Lambda_c^+ \rightarrow \Lambda K^+) = (6.1 \pm 1.2) \times 10^{-4}$ within 1σ and $\mathcal{B}(\Lambda_c^+ \rightarrow \Sigma^0 K^+) = (5.2 \pm 0.8) \times 10^{-4}$ within 2σ , but with significantly improved precision.

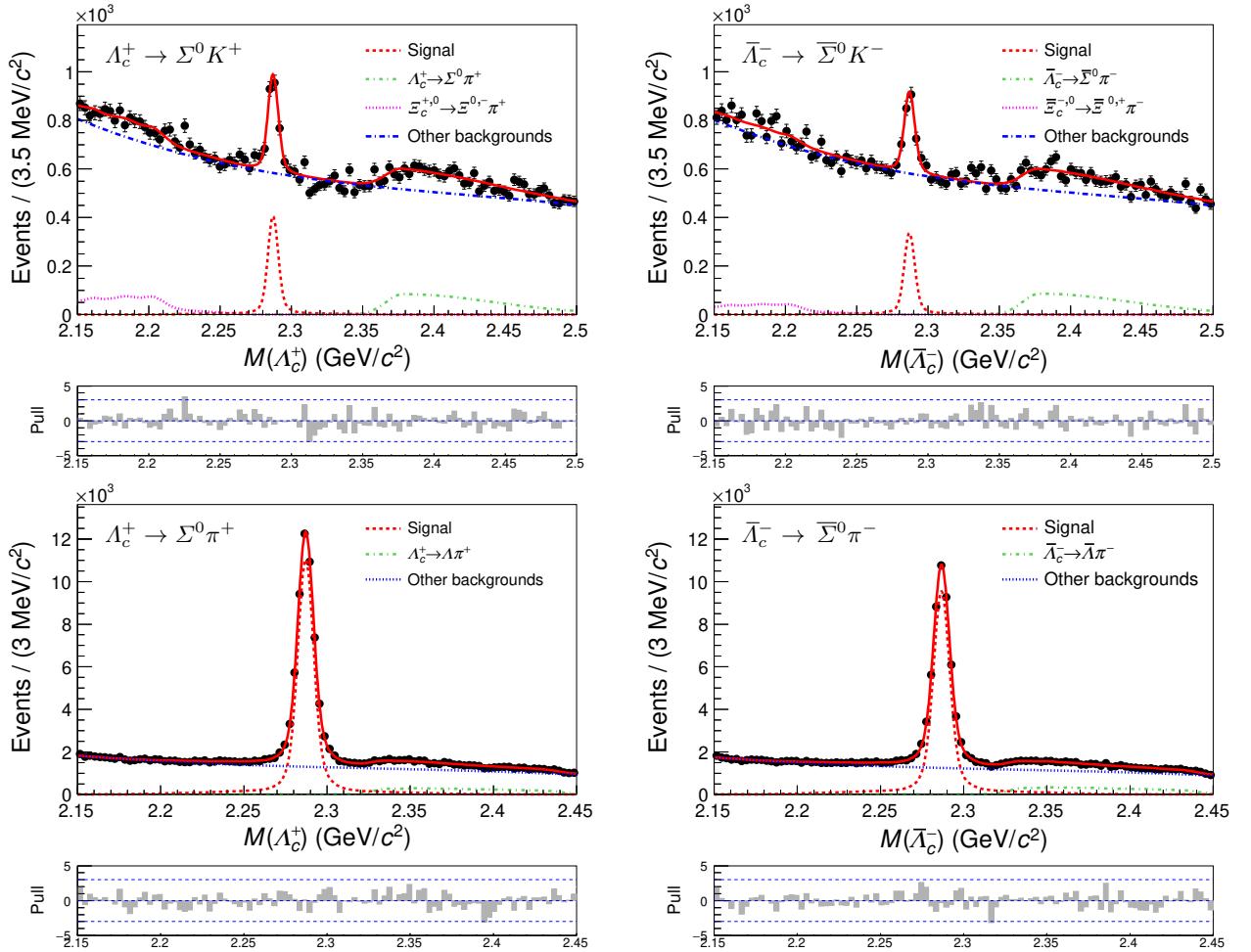


FIG. 2. The simultaneous fit to Λ_c^+ (left) and $\bar{\Lambda}_c^-$ (right) samples from real data for $\Lambda_c^+ \rightarrow \Sigma^0 K^+$ (top) and $\Lambda_c^+ \rightarrow \Sigma^0 \pi^+$ (bottom). The red curve is the total fitting result. The dashed lines show the components of signal and backgrounds (see text).

VII. DECAY ASYMMETRY PARAMETER α

To extract the α parameter, the $\cos\theta_\Lambda$ distributions of $\Lambda_c^+ \rightarrow \Lambda h^+$ modes are divided into 10 bins of uniform width. The $\cos\theta_{\Sigma^0}$ versus $\cos\theta_\Lambda$ distributions for $\Lambda_c^+ \rightarrow \Sigma^0 h^+$ modes are similarly divided into 5×5 bins for $\Lambda_c^+ \rightarrow \Sigma^0 K^+$ and 6×6 bins for $\Lambda_c^+ \rightarrow \Sigma^0 \pi^+$, since the latter mode has much greater statistics. To extract the per-bin yield, we fit the $M(\Lambda_c^+)$ distribution with signal parameters and background polynomial parameters fixed according to the fit to the full sample integrated over helicity angles. In the $\Lambda_c^+ \rightarrow \Sigma^0 h^+$ modes, the ratio of broken- Σ^0 signal to total signal depending on the $\cos\theta_{\Sigma^0}$ bin is fixed to the truth-matched results in simulation. In the $\Lambda_c^+ \rightarrow \Sigma^0 \pi^+$ mode, the shape of the reflection background $\Lambda_c^+ \rightarrow \Lambda \pi^+$ is found to depend on the $\cos\theta_{\Sigma^0}$ bins and its shape in each bin is fixed to the results from a fit to simulation.

The fitted signal yields are corrected bin-by-bin with the signal efficiencies, which are determined based on signal MC events produced with our measured angular dis-

tribution. Here the efficiency correction has effectively included the resolution of helicity angles because the efficiencies are calculated by the ratios between the reconstructed signals in i -th bin of the cosine of reconstructed helicity angles and the generated signals in i -th bin of the cosine of helicity angles. These distributions are fitted according to Eqs. (6,7) and the fit results are shown in Fig. 3 for $\Lambda_c^+ \rightarrow \Lambda h^+$ and Fig. 4 for $\Lambda_c^+ \rightarrow \Sigma^0 h^+$. The fitted slope factors ($\alpha_{\Lambda_c^+} \alpha_\Lambda$) are

$$\alpha_{\Lambda_c^+}^{\text{avg}}(\Lambda_c^+ \rightarrow \Lambda K^+) \cdot \alpha_\Lambda^{\text{avg}} = -0.441 \pm 0.037, \quad (18)$$

$$\alpha_{\Lambda_c^+}^{\text{avg}}(\Lambda_c^+ \rightarrow \Lambda \pi^+) \cdot \alpha_\Lambda^{\text{avg}} = -0.570 \pm 0.004, \quad (19)$$

$$\alpha_{\Lambda_c^+}^{\text{avg}}(\Lambda_c^+ \rightarrow \Sigma^0 K^+) \cdot \alpha_\Lambda^{\text{avg}} = -0.41 \pm 0.14, \quad (20)$$

$$\alpha_{\Lambda_c^+}^{\text{avg}}(\Lambda_c^+ \rightarrow \Sigma^0 \pi^+) \cdot \alpha_\Lambda^{\text{avg}} = -0.349 \pm 0.012, \quad (21)$$

where only statistical uncertainties are given. The superscript ‘avg’ denotes the averaged α value for the combined Λ_c^+ (Λ) and $\bar{\Lambda}_c^-$ ($\bar{\Lambda}$) decays. Dividing these results by the most precise $\alpha_\Lambda^{\text{avg}} = 0.7542 \pm 0.0026$ from BESIII [18] gives the final decay asymmetry parameters

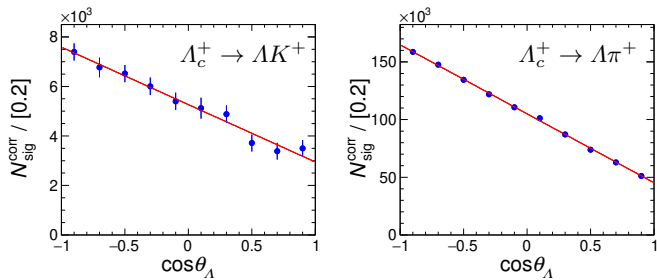


FIG. 3. The $\cos\theta_A$ distributions of $\Lambda_c^+ \rightarrow \Lambda K^+$ and $\Lambda_c^+ \rightarrow \Lambda\pi^+$ and their conjugated decays after efficiency corrections. The red curves show the fitted results with the χ^2 divided by the number of degree of freedom, $\chi^2/9 = 0.43$ and 1.05 , respectively.

$\alpha_{\Lambda_c^+}^{\text{avg}}$ for the combined Λ_c^+ and $\bar{\Lambda}_c^-$ sample,

$$\alpha_{\Lambda_c^+}^{\text{avg}}(\Lambda_c^+ \rightarrow \Lambda K^+) = -0.585 \pm 0.049 \pm 0.018, \quad (22)$$

$$\alpha_{\Lambda_c^+}^{\text{avg}}(\Lambda_c^+ \rightarrow \Lambda\pi^+) = -0.755 \pm 0.005 \pm 0.003, \quad (23)$$

$$\alpha_{\Lambda_c^+}^{\text{avg}}(\Lambda_c^+ \rightarrow \Sigma^0 K^+) = -0.54 \pm 0.18 \pm 0.09, \quad (24)$$

$$\alpha_{\Lambda_c^+}^{\text{avg}}(\Lambda_c^+ \rightarrow \Sigma^0\pi^+) = -0.463 \pm 0.016 \pm 0.008, \quad (25)$$

where the first uncertainties are statistical and the second are systematic, which are described in detail in Sec. IX. The measured values of $\alpha_{\Lambda_c^+}^{\text{avg}}$ for the $\Lambda_c^+ \rightarrow \Lambda K^+$ and $\Lambda_c^+ \rightarrow \Sigma^0 K^+$ modes are the first α results for SCS decays of charmed baryons. The measured values of $\alpha_{\Lambda_c^+}^{\text{avg}}$ for the $\Lambda_c^+ \rightarrow \Lambda\pi^+$ and $\Lambda_c^+ \rightarrow \Sigma^0\pi^+$ modes are consistent with the current world average values: $\alpha_{\Lambda_c^+}^{\text{avg}}(\Lambda_c^+ \rightarrow \Lambda\pi^+) = -0.84 \pm 0.09$ [38] and $\alpha_{\Lambda_c^+}^{\text{avg}}(\Lambda_c^+ \rightarrow \Sigma^0\pi^+) = -0.73 \pm 0.18$ [58], but with significantly improved precision: the uncertainty is improved from 11% to 1% for $\alpha_{\Lambda_c^+}^{\text{avg}}(\Lambda_c^+ \rightarrow \Lambda\pi^+)$ and from 18% to 4% for $\alpha_{\Lambda_c^+}^{\text{avg}}(\Lambda_c^+ \rightarrow \Sigma^0\pi^+)$.

VIII. α -INDUCED CP ASYMMETRY

We separate the Λ_c^+ and $\bar{\Lambda}_c^-$ samples and measure $\alpha_{\Lambda_c^+}$ and $\alpha_{\bar{\Lambda}_c^-}$ with the same method described above. The signal shape parameters for individual bins of helicity angles are fixed to the fitted results in the full sample integrated over helicity angles for Λ_c^+ and $\bar{\Lambda}_c^-$ separately. The helicity angle distributions for the Λ_c^+ and $\bar{\Lambda}_c^-$ samples are fitted separately, and the fitted slope factors, $\alpha_{\Lambda_c^+}\alpha_-$ and $\alpha_{\bar{\Lambda}_c^-}\alpha_+$, are listed in Table II. Additional details are given in the supplemental materials.

Using the precise results $\alpha_-(\Lambda \rightarrow p\pi^-) = 0.7519 \pm 0.0043$ and $\alpha_+(\bar{\Lambda} \rightarrow \bar{p}\pi^+) = -0.7559 \pm 0.0047$ measured by BESIII [18], we extract four α -induced CP asymmetries as listed in Table II, where A_{CP}^α for $\Lambda_c^+ \rightarrow \Lambda K^+$, $\Lambda_c^+ \rightarrow \Sigma^0 K^+$, and $\Lambda_c^+ \rightarrow \Sigma^0\pi^+$ are measured for the first

time. The measured A_{CP}^α for $\Lambda_c^+ \rightarrow \Lambda\pi^+$ is consistent with previous results, but with much better precision.

We search for hyperon CPV in $\Lambda \rightarrow p\pi^-$ in CF modes. Using the fitted slopes $\alpha_{\Lambda_c^+}\alpha_-$ and $\alpha_{\bar{\Lambda}_c^-}\alpha_+$ for $\Lambda_c^+ \rightarrow \Lambda\pi^+$ and $\Lambda_c^+ \rightarrow \Sigma^0\pi^+$ as listed in Table II, the α -induced CP asymmetry of $\Lambda \rightarrow p\pi^-$ is measured to be $+0.0169 \pm 0.0073 \pm 0.0120$ in $\Lambda_c^+ \rightarrow \Lambda\pi^+$ and $-0.026 \pm 0.034 \pm 0.030$ in $\Lambda_c^+ \rightarrow \Sigma^0\pi^+$. Finally, their average value is calculated to be

$$A_{CP}^\alpha(\Lambda \rightarrow p\pi^-) = +0.013 \pm 0.007 \pm 0.011. \quad (26)$$

This is the first measurement of hyperon CPV searches in CF charm decays. No evidence of Λ -hyperon CPV is found.

IX. SYSTEMATIC UNCERTAINTIES

Most of the systematic uncertainties for the direct CP asymmetry cancel since they affect both Λ_c^+ and $\bar{\Lambda}_c^-$ decays. The remaining systematic uncertainties are listed in Table IV. The uncertainty due to each charged track asymmetry map is evaluated by varying the asymmetry value bin-by-bin by its uncertainty ($\pm 1\sigma$) and repeating the measurement of the A_{CP}^{dir} . The resulting deviations from the nominal A_{CP}^{dir} value are added in quadrature for positive and negative shifts, separately, and assigned as a systematic uncertainty. We sample the parameters of the signal PDF, which are fixed in the nominal fit, from a multivariate Gaussian distribution that accounts for their uncertainties and correlations and re-fit for the signal yield. The procedure is repeated 1000 times, and the root-mean-square of the distribution of fitted yields is taken as the systematic uncertainty due to the fixed parameters. To allow for the different background shapes for the Λ_c^+ and $\bar{\Lambda}_c^-$ candidates, the background parameters are allowed to differ. The difference in the fitted results relative to the nominal results are assigned as a systematic uncertainty. We consider the possible fit bias with a linearity test for A_{CP}^{dir} with toy MC samples which are generated with five $A_{\text{raw}}^{\text{corr}}$ values per channel. A linear fit is applied to the measured $A_{\text{raw}}^{\text{corr}}$ distribution versus the generated values. The fitted slopes consistent with one indicate no fit bias. The relative shift between the fitted linear function and the nominal value is taken as a systematic uncertainty. The remaining asymmetry due to the reconstruction of the Λ or its children is considered as follows. The reference modes are weighted based on the ratio of the shapes for the momentum and polar angle of the Λ between the signal and reference modes, causing the distributions in the reference modes to be the same as those for the signal modes. After this weighting, $A_{\text{raw}}^{\text{corr}}$ is remeasured and A_{CP}^{dir} is calculated. The changes on A_{CP}^{dir} are -0.02% for $\Lambda_c^+ \rightarrow \Lambda K^+$ and -0.04% for $\Lambda_c^+ \rightarrow \Sigma^0 K^+$, which are assigned as system-

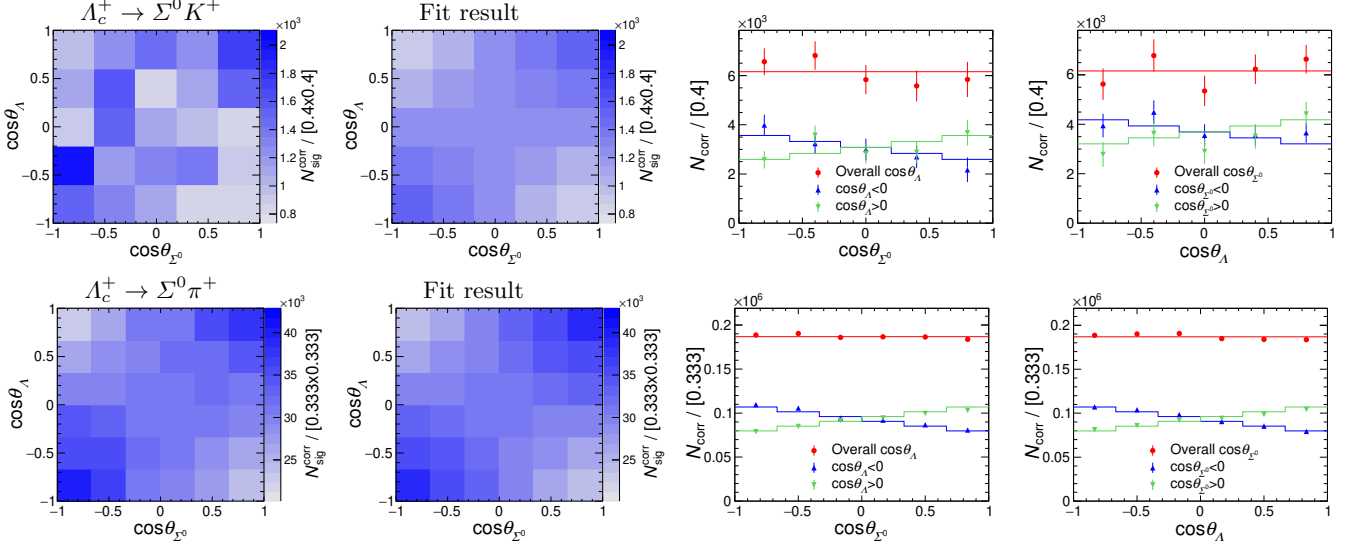


FIG. 4. The first column shows the $[\cos\theta_{\Sigma^0}, \cos\theta_{\Lambda}]$ distributions of $\Lambda_c^+ \rightarrow \Sigma^0 K^+$ and $\Lambda_c^+ \rightarrow \Sigma^0 \pi^+$ and their conjugated decays after efficiency correction; the second column shows the fitted results of the first column with the χ^2 divided by the number of degree of freedom $\chi^2/24 = 0.87$ for $\Lambda_c^+ \rightarrow \Sigma^0 K^+$ and $\chi^2/35 = 1.45$ for $\Lambda_c^+ \rightarrow \Sigma^0 \pi^+$. The third column shows the projections of the $\cos\theta_{\Sigma^0}$ distributions (point with error) and the fit results (histograms) in overall (red) or negative (blue) or positive (green) $\cos\theta_{\Lambda}$ region; vice versa in fourth column. The absolute slopes of all projections in slices equal half of the fitted slope mentioned in text.

TABLE II. The fitted slopes $\alpha_{\Lambda_c^\pm \alpha_\mp}$ for Λ_c^+ and $\bar{\Lambda}_c^-$ samples, and decay asymmetry parameters $\alpha_{\Lambda_c^+}$ and $\alpha_{\bar{\Lambda}_c^-}$ for individual Λ_c^+ and $\bar{\Lambda}_c^-$ samples using the most precise α_\mp from BESIII recently [18], and the corresponding α -induced CP asymmetry A_{CP}^α , comparing with current world averages (W.A.) [38].

Channel	$\alpha_{\Lambda_c^+ \alpha_-}$	$\alpha_{\Lambda_c^- \alpha_+}$	$\alpha_{\Lambda_c^+}$	$\alpha_{\bar{\Lambda}_c^-}$	A_{CP}^α	W.A. A_{CP}^α
$\Lambda_c^+ \rightarrow \Lambda K^+$	-0.425 ± 0.053	-0.448 ± 0.053	$-0.566 \pm 0.071 \pm 0.028$	$0.592 \pm 0.070 \pm 0.079$	$-0.023 \pm 0.086 \pm 0.071$	-
$\Lambda_c^+ \rightarrow \Lambda \pi^+$	-0.590 ± 0.006	-0.570 ± 0.006	$-0.784 \pm 0.008 \pm 0.006$	$0.754 \pm 0.008 \pm 0.018$	$+0.020 \pm 0.007 \pm 0.014$	-0.07 ± 0.22
$\Lambda_c^+ \rightarrow \Sigma^0 K^+$	-0.43 ± 0.18	-0.37 ± 0.21	$-0.58 \pm 0.24 \pm 0.09$	$0.49 \pm 0.28 \pm 0.14$	$+0.08 \pm 0.35 \pm 0.14$	-
$\Lambda_c^+ \rightarrow \Sigma^0 \pi^+$	-0.340 ± 0.016	-0.358 ± 0.017	$-0.452 \pm 0.022 \pm 0.023$	$0.473 \pm 0.023 \pm 0.035$	$-0.023 \pm 0.034 \pm 0.030$	-

atic uncertainty. The total systematic uncertainty is determined from the sum of all contributions in quadrature to be ${}_{-0.7}^{+1.2} \times 10^{-3}$ for $A_{CP}^{\text{dir}}(\Lambda_c^+ \rightarrow \Lambda K^+)$ and ${}_{-4.3}^{+3.0} \times 10^{-3}$ for $A_{CP}^{\text{dir}}(\Lambda_c^+ \rightarrow \Sigma^0 K^+)$. And considering the statistical uncertainties of A_{CP}^{dir} results are larger than 1%, we assign 0.1% and 0.4% as the final systematic uncertainties of $A_{CP}^{\text{dir}}(\Lambda_c^+ \rightarrow \Lambda K^+)$ and $A_{CP}^{\text{dir}}(\Lambda_c^+ \rightarrow \Sigma^0 K^+)$, respectively, which are greatly smaller than the corresponding statistical uncertainties 2.6% and 5.4%.

TABLE III. The absolute systematic uncertainties (in units of 10^{-3}) for CP asymmetry A_{CP}^{dir} .

Sources	$A_{CP}^{\text{dir}}(\Lambda_c^+ \rightarrow \Lambda K^+)$	$A_{CP}^{\text{dir}}(\Lambda_c^+ \rightarrow \Sigma^0 K^+)$
$A_\epsilon^{K^+}$ map	$+0.8$ -0.2	± 0.4
$A_\epsilon^{\pi^+}$ map	± 0.4	$+0.5$ -2.5
Signal shape	± 0.5	± 1.4
Background shape	-0.2	-3.1
Fit bias	$+0.6$	$+2.6$
Λ asymmetry	-0.2	-0.4
Total	$+1.2$ -0.7	$+3.0$ -4.3

For the measurement of BF ratio, most systematic uncertainties cancel since they affect both the signal and reference modes. The remaining systematic uncertainties are listed in Table IV. Using the $D^{*+} \rightarrow [D^0 \rightarrow K^- \pi^+] \pi^+$ control sample, the PID uncertainties are estimated to be 0.9% for $\Lambda_c^+ \rightarrow \Lambda K^+$, 0.8% for $\Lambda_c^+ \rightarrow \Lambda \pi^+$, 0.9% for $\Lambda_c^+ \rightarrow \Sigma^0 K^+$, and 0.8% for $\Lambda_c^+ \rightarrow \Sigma^0 \pi^+$. Since the kaon and pion PID efficiency use the same control sample, we assign 1.7% as the systematic uncertainty for both BF ratios. The systematic uncertainties associated with the fixed parameters in the signal-yield fit is determined according to the same method as for A_{CP}^{dir} to be 0.2% and 0.4% for the Λ - and Σ^0 -involved modes, respectively. In modes that include a Σ^0 , the broken- Σ^0 signal has a fixed ratio to signal based on MC simulation. The $M(\Lambda_c^+)$ distributions of the MC sample and experimental data in $M(\Sigma^0)$ sideband region have nearly same shapes, which suggests that the MC simulation is reliable for this broken- Σ^0 signal. We vary its ratio in the $M(\Lambda_c^+)$ fit by $\pm 10\%$ and the larger deviation, 0.1%, is assigned as a conservative estimate. We consider the effects of the Ξ_c background shape in the $\Lambda_c^+ \rightarrow \Sigma^0 \pi^+$ mode by pa-

TABLE IV. Relative systematic uncertainties (in units of %) for branching fractions.

Sources	$\frac{\mathcal{B}(\Lambda_c^+ \rightarrow \Lambda K^+)}{\mathcal{B}(\Lambda_c^+ \rightarrow \Lambda \pi^+)}$	$\frac{\mathcal{B}(\Lambda_c^+ \rightarrow \Sigma^0 K^+)}{\mathcal{B}(\Lambda_c^+ \rightarrow \Sigma^0 \pi^+)}$
	PID efficiency correction	1.7
Signal shape	0.2	0.4
Background shape	–	0.1
BCS effect	0.1	0.4
Efficiency ratio	0.2	0.4
Total	1.7	1.8

parameterizing it separately from the other backgrounds. The difference in the fitted signal yield is 0.1%, assigned as a systematic uncertainty. Since the multiplicity of events for modes that include a Λ is small, we remove events with multiple candidates and repeat the measurement. For modes that include a Σ^0 , an alternative BCS method is applied to select the candidate with highest momentum γ from the Σ^0 decay. The resulting changes in the branching fraction measurement are assigned as systematic uncertainties. The α value used in signal MC production is varied by its uncertainty and the resulting change in the efficiency is assigned as a systematic uncertainty. A systematic uncertainty due to limited MC statistics is also considered. The total systematic uncertainty is determined by adding the uncertainties from all sources in quadrature, as given in Table IV.

For the α and A_{CP}^α measurements, we consider the systematic uncertainty due to the number of helicity angle bins, the efficiency curve, the fit bias, and the quoted uncertainty on α_\mp . We change the number of helicity angle bins from 10 to 8 or 12 for $\Lambda_c^+ \rightarrow \Lambda h^+$, from 5×5 to 4×4 or 6×6 for $\Lambda_c^+ \rightarrow \Sigma^0 K^+$, and from 6×6 to 5×5 or 7×7 for $\Lambda_c^+ \rightarrow \Sigma^0 \pi^+$. The α value used in signal MC production is varied by its uncertainty. The resulting changes in α or A_{CP}^α are assigned as systematic uncertainties. Additional signal MC samples are produced with different hypotheses for the Λ_c^+ polarization ($\mathbf{P} = \pm 0.4$), which may affect the efficiency as a function of helicity angle [59]. The maximum difference in the measured α relative to the unpolarized hypothesis, 0.001, is taken as a systematic uncertainty. We consider the possible fit bias for α and A_{CP}^α with a linearity test, in which we replace the signal events in the MC sample with events produced with a special angular distribution using five α values. A linear fit is applied to the measured α distribution versus the generated values. The fitted slopes consistent with one indicate no fit bias. The relative shift between the fitted linear function and the nominal value is taken as a systematic uncertainty. The quoted uncertainties of α_A^{avg} and α_\mp (with their correlation coefficient $\rho(\alpha_-, \alpha_+) = 0.850$ [18] considered) of $\Lambda \rightarrow p\pi^-$ decays are assigned as systematic uncertainties. The effect arising from the spin precession of Λ -hyperons with average momentum 2 GeV/ c in the magnetic field of the detector (1.5 T) has been considered. The resulting systematic uncertainty is estimated

at level of $\mathcal{O}(10^{-4})$ [60], which is negligible given the precision of this result. The total systematic uncertainties for $\alpha_{\text{avg}}/\alpha_{\Lambda_c^+}/\alpha_{\Lambda_c^-}/A_{CP}^\alpha/A_{CP}^\alpha(\Lambda)$ are taken as the sum in quadrature of all contributions, as listed in Table V.

X. SUMMARY

In conclusion, based on the 980 fb $^{-1}$ data set collected with the Belle detector, we make the first measurement of the direct CP asymmetry in SCS two-body decays of charmed baryons, $A_{CP}^{\text{dir}}(\Lambda_c^+ \rightarrow \Lambda K^+) = +0.021 \pm 0.026 \pm 0.001$ and $A_{CP}^{\text{dir}}(\Lambda_c^+ \rightarrow \Sigma^0 K^+) = +0.025 \pm 0.054 \pm 0.004$. The relative branching fractions are measured to be, $\mathcal{B}(\Lambda_c^+ \rightarrow \Lambda K^+)/\mathcal{B}(\Lambda_c^+ \rightarrow \Lambda \pi^+) = (5.05 \pm 0.13 \pm 0.09)\%$ and $\mathcal{B}(\Lambda_c^+ \rightarrow \Sigma^0 K^+)/\mathcal{B}(\Lambda_c^+ \rightarrow \Sigma^0 \pi^+) = (2.78 \pm 0.15 \pm 0.05)\%$, which supersede previous Belle measurements [39]. Using the world average values for the branching fractions for $\Lambda_c^+ \rightarrow (\Lambda, \Sigma^0)\pi^+$, we obtain $\mathcal{B}(\Lambda_c^+ \rightarrow \Lambda K^+) = (6.57 \pm 0.17 \pm 0.11 \pm 0.35) \times 10^{-4}$ and $\mathcal{B}(\Lambda_c^+ \rightarrow \Sigma^0 K^+) = (3.58 \pm 0.19 \pm 0.06 \pm 0.19) \times 10^{-4}$. These results are the most precise to date and significantly improve the precision of the world average values [38].

We obtain the averaged decay asymmetry parameters $\alpha_{\Lambda_c^+}^{\text{avg}}(\Lambda_c^+ \rightarrow \Lambda K^+) = -0.585 \pm 0.049 \pm 0.018$ and $\alpha_{\Lambda_c^+}^{\text{avg}}(\Lambda_c^+ \rightarrow \Sigma^0 K^+) = -0.54 \pm 0.18 \pm 0.09$ for the first time. We obtain $\alpha_{\Lambda_c^+}^{\text{avg}}(\Lambda_c^+ \rightarrow \Lambda \pi^+) = -0.755 \pm 0.005 \pm 0.003$ and $\alpha_{\Lambda_c^+}^{\text{avg}}(\Lambda_c^+ \rightarrow \Sigma^0 \pi^+) = -0.463 \pm 0.016 \pm 0.008$, which are consistent with previous measurements [38] but with significantly improved precision. We also determine the α -parameter for Λ_c^+ and Λ_c^- individually and search for CPV via the α -induced CP asymmetry, as listed in Table II. These results include the first measurements of A_{CP}^α for SCS decays of charmed baryons, $A_{CP}^\alpha(\Lambda_c^+ \rightarrow \Lambda K^+) = -0.023 \pm 0.086 \pm 0.071$ and $A_{CP}^\alpha(\Lambda_c^+ \rightarrow \Sigma^0 K^+) = +0.08 \pm 0.35 \pm 0.14$. We search for Λ hyperon CPV via the α -induced CP asymmetry in $\Lambda_c^+ \rightarrow \Lambda \pi^+$ and $\Lambda_c^+ \rightarrow \Sigma^0 \pi^+$ decays, and determine $A_{CP}^\alpha(\Lambda \rightarrow p\pi^-) = +0.013 \pm 0.007 \pm 0.011$ by combining the two modes. No evidence of baryon CPV is found. The method used in our $A_{CP}^\alpha(\Lambda \rightarrow p\pi^-)$ measurement can be applied to other hyperons, such as $A_{CP}^\alpha(\Xi^{0,-} \rightarrow \Lambda \pi^{0,-})$ in $\Lambda_c^+ \rightarrow \Xi^0 K^+$ and $\Xi_c^{+,0} \rightarrow \Xi^{0,-} \pi^+$. Our measurement is a milestone for hyperon CPV searches in charm CF decays and this method is promising for precise measurements of various hyperon CPV at Belle II and LHCb.

CONFLICT OF INTEREST

The authors declare that they have no conflict of interest.

TABLE V. Absolute systematic uncertainties (in units of 10^{-2}) for decay asymmetry parameters and the α -induced CP asymmetries: $\alpha_{\text{avg}}/\alpha_{\Lambda_c^+}/\alpha_{\Lambda_c^-}/A_{CP}^\alpha$ in each decay mode (the fifth items in $\Lambda_c^+ \rightarrow \Lambda\pi^+/\Sigma^0\pi^+$ are for $A_{CP}^\alpha(\Lambda)$).

Sources	$\Lambda_c^+ \rightarrow \Lambda K^+$	$\Lambda_c^+ \rightarrow \Lambda\pi^+$	$\Lambda_c^+ \rightarrow \Sigma^0 K^+$	$\Lambda_c^+ \rightarrow \Sigma^0\pi^+$
$\cos\theta$ bins	0.8/1.5/1.5/1.4	0.0/0.1/0.2/0.2/0.16	7.4/6.9/ 9.9/ 8.4	0.7/1.5/3.3/1.9/1.9
Efficiency curve	0.2/0.5/0.1/0.4	0.2/0.3/0.1/0.3/0.29	1.4/1.1/ 1.8/ 0.9	0.1/0.5/0.4/0.9/0.9
Fit bias	1.6/2.3/7.7/6.9	0.2/0.3/1.7/1.2/1.15	4.1/5.7/10.3/11.7	0.4/1.7/0.9/2.1/2.1
$\alpha_\mp(\Lambda \rightarrow p\pi^-)$	0.2/0.3/0.4/0.6	0.2/0.4/0.5/0.6/-	0.2/0.3/ 0.3/ 0.6	0.1/0.2/0.3/0.6/-
Total	1.8/2.8/7.9/7.1	0.3/0.6/1.8/1.4/1.20	8.6/9.0/14.4/14.4	0.8/2.3/3.5/3.0/3.0

ACKNOWLEDGMENTS

This work, based on data collected using the Belle detector, which was operated until June 2010, was supported by the Ministry of Education, Culture, Sports, Science, and Technology (MEXT) of Japan, the Japan Society for the Promotion of Science (JSPS), and the Tau-Lepton Physics Research Center of Nagoya University; the Australian Research Council including grants DP180102629, DP170102389, DP170102204, DE220100462, DP150103061, FT130100303; Austrian Federal Ministry of Education, Science and Research (FWF) and FWF Austrian Science Fund No. P 31361-N36; the National Natural Science Foundation of China under Contracts No. 11675166, No. 11705209; No. 11805064; No. 11975076; No. 12135005; No. 12175041; No. 12161141008; Key Research Program of Frontier Sciences, Chinese Academy of Sciences (CAS), Grant No. QYZDJ-SSW-SLH011; the Shanghai Science and Technology Committee (STCSM) under Grant No. 19ZR1403000; the Ministry of Education, Youth and Sports of the Czech Republic under Contract No. LTT17020; the Czech Science Foundation Grant No. 22-18469S; Horizon 2020 ERC Advanced Grant No. 884719 and ERC Starting Grant No. 947006 ‘‘Inter-Leptons’’ (European Union); the Carl Zeiss Foundation, the Deutsche Forschungsgemeinschaft, the Excellence Cluster Universe, and the VolkswagenStiftung; the Department of Atomic Energy (Project Identification No. RTI 4002) and the Department of Science and Technology of India; the Istituto Nazionale di Fisica Nucleare of Italy; National Research Foundation (NRF) of Korea Grant Nos. 2016R1D1A1B02012900, 2018R1A2B-3003643, 2018R1A6A1A06024970, RS202200197659, 2019R1I1A3A01058933, 2021R1A6A1A03043957, 2021R1F1A1060423, 2021R1F1A1064008, 2022R1A2C-1003993; Radiation Science Research Institute, Foreign Large-size Research Facility Application Supporting project, the Global Science Experimental Data Hub Center of the Korea Institute of Science and Technology Information and KREONET/GLORIAD; the Polish Ministry of Science and Higher Education and the National Science Center; the Ministry of Science and Higher Education of the Russian Federation, Agreement

14.W03.31.0026, and the HSE University Basic Research Program, Moscow; University of Tabuk research grants S-1440-0321, S-0256-1438, and S-0280-1439 (Saudi Arabia); the Slovenian Research Agency Grant Nos. J1-9124 and P1-0135; Ikerbasque, Basque Foundation for Science, Spain; the Swiss National Science Foundation; the Ministry of Education and the Ministry of Science and Technology of Taiwan; and the United States Department of Energy and the National Science Foundation. These acknowledgements are not to be interpreted as an endorsement of any statement made by any of our institutes, funding agencies, governments, or their representatives. We thank the KEKB group for the excellent operation of the accelerator; the KEK cryogenics group for the efficient operation of the solenoid; and the KEK computer group and the Pacific Northwest National Laboratory (PNNL) Environmental Molecular Sciences Laboratory (EMSL) computing group for strong computing support; and the National Institute of Informatics, and Science Information Network 6 (SINET6) for valuable network support. We warmly thank Fu-Sheng Yu, Di Wang, Chao-Qiang Geng, Chia-Wei Liu, and Xian-Wei Kang for valuable and helpful discussions.

-
- [1] A.D. Sakharov, *Violation of CP Invariance, C asymmetry, and baryon asymmetry of the universe*, *Pisma Zh. Eksp. Teor. Fiz.* **5** (1967) 32.
 - [2] A.D. Sakharov, *Baryon asymmetry of the universe*, *Sov. Phys. Usp.* **34** (1991) 417.
 - [3] M.E. Shaposhnikov, *Baryon Asymmetry of the Universe in Standard Electroweak Theory*, *Nucl. Phys. B* **287** (1987) 757.
 - [4] J. Brod, A.L. Kagan and J. Zupan, *Size of direct CP violation in singly Cabibbo-suppressed D decays*, *Phys. Rev. D* **86** (2012) 014023.
 - [5] H.-n. Li, C.-D. Lu and F.-S. Yu, *Branching ratios and direct CP asymmetries in D → PP decays*, *Phys. Rev. D* **86** (2012) 036012.
 - [6] H.-Y. Cheng and C.-W. Chiang, *Revisiting CP violation in D → PP and VP decays*, *Phys. Rev. D* **100** (2019) 093002.
 - [7] A.L. Kagan and L. Silvestrini, *Dispersive and absorptive CP violation in D⁰- \bar{D}^0 mixing*, *Phys. Rev. D* **103**



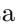







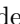
- (2021) 053008.
- [8] H.-Y. Cheng and C.-W. Chiang, *CP violation in quasi-two-body $D \rightarrow VP$ decays and three-body D decays mediated by vector resonances*, *Phys. Rev. D* **104** (2021) 073003.
- [9] D. Delepine, G. Faisel and C.A. Ramirez, *Direct CP violation in $D^+ \rightarrow K^0(\bar{K}^0)\pi^+$ decays as a probe for new physics*, *Eur. Phys. J. C* **80** (2020) 596.
- [10] A. Dery and Y. Nir, *Implications of the LHCb discovery of CP violation in charm decays*, *JHEP* **12** (2019) 104.
- [11] M. Chala, A. Lenz, A.V. Rusov and J. Scholtz, *ΔA_{CP} within the Standard Model and beyond*, *JHEP* **07** (2019) 161.
- [12] M. Saur and F.-S. Yu, *Charm CPV: observation and prospects*, *Sci. Bull.* **65** (2020) 1428.
- [13] LHCb Collaboration, R. Aaij et al., *Observation of CP Violation in Charm Decays*, *Phys. Rev. Lett.* **122** (2019) 211803.
- [14] LHCb Collaboration, R. Aaij et al., *A measurement of the CP asymmetry difference in $\Lambda_c^+ \rightarrow pK^-K^+$ and $p\pi^-\pi^+$ decays*, *J. High Energy. Phys.* **2018** (2018) 182.
- [15] LHCb Collaboration, R. Aaij et al., *Search for CP violation in $\Xi_c^+ \rightarrow pK^-\pi^+$ decays using model-independent techniques*, *Eur. Phys. J. C* **80** (2020) 986.
- [16] T.D. Lee and C.-N. Yang, *General Partial Wave Analysis of the Decay of a Hyperon of Spin 1/2*, *Phys. Rev.* **108** (1957) 1645.
- [17] FOCUS Collaboration, J.M. Link et al., *Study of the decay asymmetry parameter and CP violation parameter in the $\Lambda_c^+ \rightarrow \Lambda\pi^+$ decay*, *Phys. Lett. B* **634** (2006) 165.
- [18] BESIII Collaboration, M. Ablikim et al., *Precise Measurements of Decay Parameters and CP Asymmetry with Entangled $\Lambda\bar{\Lambda}$ Pairs*, *Phys. Rev. Lett.* **129** (2022) 131801.
- [19] J.F. Donoghue and S. Pakvasa, *Signals of CP Nonconservation in Hyperon Decay*, *Phys. Rev. Lett.* **55** (1985) 162.
- [20] J.F. Donoghue, X.-G. He and S. Pakvasa, *Hyperon Decays and CP Nonconservation*, *Phys. Rev. D* **34** (1986) 833.
- [21] J. Tandean and G. Valencia, *CP violation in hyperon nonleptonic decays within the standard model*, *Phys. Rev. D* **67** (2003) 056001.
- [22] N. Salone, P. Adlarson, V. Batzskaya, A. Kupsc, S. Leupold and J. Tandean, *Study of CP violation in hyperon decays at super-charm-tau factories with a polarized electron beam*, *Phys. Rev. D* **105** (2022) 116022.
- [23] D. Chang, X.-G. He and S. Pakvasa, *CP violation in hyperon decays due to left-right mixing*, *Phys. Rev. Lett.* **74** (1995) 3927.
- [24] X.-G. He, H. Murayama, S. Pakvasa and G. Valencia, *CP violation in hyperon decays from supersymmetry*, *Phys. Rev. D* **61** (2000) 071701.
- [25] C.-H. Chen, *CP violation in hyperon decays from SUSY with Hermitian Yukawa and A matrices*, *Phys. Lett. B* **521** (2001) 315.
- [26] J. Tandean, *New physics and CP violation in hyperon nonleptonic decays*, *Phys. Rev. D* **69** (2004) 076008.
- [27] J.-P. Wang and F.-S. Yu, *Probing hyperon CP violation from charm baryon decays*, **2208.01589**.
- [28] T. Uppal, R.C. Verma and M.P. Khanna, *Constituent quark model analysis of weak mesonic decays of charm baryons*, *Phys. Rev. D* **49** (1994) 3417.
- [29] H.-Y. Cheng, X.-W. Kang and F. Xu, *Singly Cabibbo-suppressed hadronic decays of Λ_c^+* , *Phys. Rev. D* **97** (2018) 074028.
- [30] J. Zou, F. Xu, G. Meng and H.-Y. Cheng, *Two-body hadronic weak decays of antitriplet charmed baryons*, *Phys. Rev. D* **101** (2020) 014011.
- [31] C.Q. Geng, C.-W. Liu and T.-H. Tsai, *Asymmetries of anti-triplet charmed baryon decays*, *Phys. Lett. B* **794** (2019) 19.
- [32] L.-L. Wang and F. Wilczek, *$SU(3)$ Predictions for Charmed Meson Decays*, *Phys. Rev. Lett.* **43** (1979) 816.
- [33] M.J. Savage and R.P. Springer, *$SU(3)$ Predictions for Charmed Baryon Decays*, *Phys. Rev. D* **42** (1990) 1527.
- [34] K.K. Sharma and R.C. Verma, *$SU(3)$ flavor analysis of two-body weak decays of charmed baryons*, *Phys. Rev. D* **55** (1997) 7067.
- [35] C.-D. Lü, W. Wang and F.-S. Yu, *Test flavor $SU(3)$ symmetry in exclusive Λ_c decays*, *Phys. Rev. D* **93** (2016) 056008.
- [36] R. Koniuk and N. Isgur, *Baryon Decays in a Quark Model with Chromodynamics*, *Phys. Rev. D* **21** (1980) 1868.
- [37] H.-Y. Cheng, *Charmed Baryon Physics Circa 2021*, *Chin. J. Phys.* **78** (2022) 324.
- [38] Particle Data Group, R.L. Workman et al., *Review of Particle Physics*, *Prog. Theo. Exp. Phys.* **2022** (2022) 083C01.
- [39] Belle Collaboration, K. Abe et al., *Observation of Cabibbo suppressed and W exchange Λ_c^+ baryon decays*, *Phys. Lett. B* **524** (2002) 33.
- [40] BaBar Collaboration, B. Aubert et al., *Measurements of Λ_c^+ branching fractions of Cabibbo-suppressed decay modes involving Λ and Σ^0* , *Phys. Rev. D* **75** (2007) 052002.
- [41] Belle Collaboration, A. Abashian et al., *The Belle Detector*, *Nucl. Instrum. Meth. A* **479** (2002) 117.
- [42] Belle Collaboration, J. Brodzicka et al., *Physics Achievements from the Belle Experiment*, *Prog. Theo. Exp. Phys.* **2012** (2012) 04D001.
- [43] S. Kurokawa and E. Kikutani, *Overview of the KEKB accelerators*, *Nucl. Instrum. Meth. A* **499** (2003) 1.
- [44] T. Abe et al., *Achievements of KEKB*, *Prog. Theo. Exp. Phys.* **2013** (2013) 03A001.
- [45] D.J. Lange, *The EvtGen particle decay simulation package*, *Nucl. Instrum. Meth. A* **462** (2001) 152.
- [46] T. Sjöstrand, P. Edén, C. Friberg, L. Lönnblad, G. Miu, S. Mrenna et al., *High-energy physics event generation with PYTHIA 6.1*, *Comput. Phys. Commun.* **135** (2001) 238.
- [47] R. Brun et al., *GEANT3, CERN Report No. CERN-DD-EE-84-1* (1987).
- [48] E. Barberio and Z. Was, *PHOTOS: A Universal Monte Carlo for QED radiative corrections. Version 2.0*, *Comput. Phys. Commun.* **79** (1994) 291.
- [49] R.W. Brown, K.O. Mikaelian, V.K. Cung and E.A. Paschos, *Electromagnetic background in the search for neutral weak currents via $e^+e^- \rightarrow \mu^+\mu^-$* , *Phys. Lett. B* **43** (1973) 403.
- [50] R.J. Cashmore, C.M. Hawkes, B.W. Lynn and R.G. Stuart, *The Forward-Backward Asymmetry in $e^+e^- \rightarrow \mu^+\mu^-$* , *Z. Phys. C* **30** (1986) 125.
- [51] Belle Collaboration, B.R. Ko et al., *Search for CP Violation in the Decay $D^+ \rightarrow K_S^0 K^+$* , *J. High Energy.*






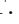


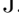


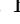
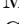

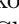
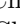



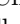


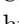














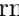
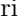


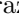


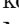
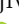
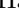
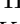


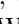
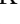



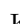




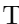




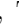

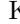



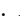






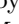


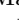
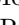
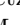
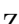


















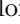
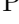

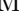

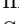
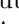

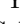

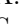

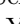






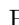
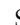





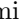
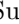


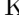






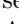
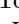
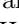
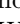







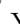


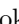
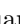


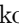














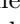
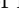
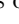
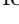
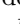
- Phys.* **2013** (2013) 098.
- [52] Belle Collaboration, B.R. Ko et al., *Evidence for CP Violation in the Decay $D^+ \rightarrow K_S^0 \pi^+$* , *Phys. Rev. Lett.* **109** (2012) 021601.
- [53] E. Nakano, *Belle PID*, *Nucl. Instrum. Meth. A* **494** (2002) 402.
- [54] K. Hanagaki, H. Kakuno, H. Ikeda, T. Iijima and T. Tsukamoto, *Electron identification in Belle*, *Nucl. Instrum. Meth. A* **485** (2002) 490.
- [55] A. Abashian et al., *Muon identification in the Belle experiment at KEKB*, *Nucl. Instrum. Meth. A* **491** (2002) 69.
- [56] BESIII Collaboration, M. Ablikim et al., *Measurement of the branching fraction of the singly Cabibbo-suppressed decay $\Lambda_c^+ \rightarrow AK^+$* , *Phys. Rev. D* **106** (2022) L111101.
- [57] BESIII Collaboration, M. Ablikim et al., *Measurement of Branching Fractions of Singly Cabibbo-suppressed Decays $\Lambda_c^+ \rightarrow \Sigma^0 K^+$ and $\Sigma^+ K_S^0$* , *Phys. Rev. D* **106** (2022) 052003.
- [58] BESIII Collaboration, M. Ablikim et al., *Measurements of Weak Decay Asymmetries of $\Lambda_c^+ \rightarrow pK_S^0$, $\Lambda\pi^+$, $\Sigma^+\pi^0$, and $\Sigma^0\pi^+$* , *Phys. Rev. D* **100** (2019) 072004.
- [59] CLEO Collaboration, P. Avery et al., *Measurement of the Λ_c decay asymmetry parameter*, *Phys. Rev. Lett.* **65** (1990) 2842.
- [60] H.-B. Li and X.-X. Ma, *Polarization difference between hyperons and antihyperons induced by an external magnetic field*, *Phys. Rev. D* **100** (2019) 076007.

THE BELLE EXPERIMENT

Belle is a first-generation “asymmetric B-factory” experiment at the KEKB asymmetric-energy e^+e^- collider in Tsukuba, Japan. Belle was designed to discover CP violation in B meson decays, as well as to cover a wide range of physics targets. Belle collected over 1 ab^{-1} of collision data between 1999 and 2010, including 772 million $B\bar{B}$ pairs produced at the energy corresponding to the $\Upsilon(4S)$ resonance. Belle has also collected large samples of data from τ -lepton, charm-, and light-hadron decays, and data at the energies of the $\Upsilon(1, 2, 3, 5S)$ resonances. In 2001, Belle observed a large CP asymmetry in B meson decays, providing strong experimental evidence for the theoretical predictions from Kobayashi and Maskawa. In 2003, Belle discovered an unexpected new charmonium-like state, $X(3872)$, heralding a new era of hadron physics. After more than a decade since the end of data-taking, Belle is still actively analyzing data and reporting new results.

THE BELLE COLLABORATION

L. K. Li , W. Shan , K. Kinoshita , I. Adachi , H. Aihara , D. M. Asner , H. Atmacan , T. Ashesh , V. Babu , S. Bahinipati , Sw. Banerjee , P.

Behera , J. Bennett , M. Bessner , V. Bhardwaj , B. Bhuyan , T. Bilka , A. Bobrov , D. Bodrov , J. Borah , M. Bračko , P. Branchini , A. Budano , M. Campajola , D. Červenkov , M.-C. Chang , P. Chang , V. Chekelian , A. Chen , B. G. Cheon , K. Chilikin , H. E. Cho , K. Cho , S.-J. Cho , S.-K. Choi , Y. Choi , S. Choudhury , D. Cinabro , N. Dash , G. De Nardo , G. De Pietro , R. Dhamija , F. Di Capua , Z. Doležal , T. V. Dong , D. Epifanov , T. Ferber , A. Frey , B. G. Fulsom , V. Gaur , A. Garmash , A. Giri , P. Goldenzweig , G. Gong , E. Graziani , T. Gu , Y. Guan , K. Gudkova , C. Hadjivasiliou , K. Hayasaka , H. Hayashii , M. T. Hedges , W.-S. Hou , C.-L. Hsu , K. Inami , A. Ishikawa , R. Itoh , W. W. Jacobs , E.-J. Jang , Q. P. Ji , S. Jia , Y. Jin , K. K. Joo , C. Kiesling , C. H. Kim , D. Y. Kim , K.-H. Kim , P. Kodyš , T. Konno , A. Korobov , S. Korpar , E. Kovalenko , P. Krokovny , T. Kuhr , R. Kumar , K. Kumara , A. Kuzmin , Y.-J. Kwon , Y.-T. Lai , T. Lam , J. S. Lange , S. C. Lee , J. Li , S. X. Li , Y. Li , Y. B. Li , L. Li Gioi , J. Libby , K. Lieret , M. Masuda , S. K. Maurya , M. Merola , F. Metzner , K. Miyabayashi , R. Mizuk , R. Mussa , M. Nakao , Z. Natkaniec , A. Natchii , L. Nayak , M. Nayak , M. Niiyama , N. K. Nisar , S. Nishida , S. Ogawa , H. Ono , P. Oskin , G. Pakhlova , S. Pardi , H. Park , S.-H. Park , A. Passeri , S. Patra , S. Paul , T. K. Pedlar , R. Pestotnik , L. E. Piiilonen , T. Podobnik , E. Prencipe , M. T. Prim , A. Rostomyan , N. Rout , G. Russo , D. Sahoo , Y. Sakai , S. Sandilya , A. Sangal , V. Savinov , G. Schnell , J. Schueler , C. Schwanda , A. J. Schwartz , Y. Seino , K. Senyo , M. E. Seviour , M. Shapkin , C. Sharma , C. P. Shen , J.-G. Shiu , J. B. Singh , A. Sokolov , E. Solovieva , M. Starič , M. Sumihama , K. Sumisawa , T. Sumiyoshi , W. Sutcliffe , M. Takizawa , U. Tamponi , K. Tanida , F. Tenchini , M. Uchida , T. Uglov , Y. Unno , S. Uno , Y. Usov , S. E. Vahsen , R. van Tonder , G. Varner , A. Vinokurova , A. Vossen , E. Waheed , E. Wang , X. L. Wang , M. Watanabe , S. Watanuki , O. Werbycka , E. Won , X. Xu , B. D. Yabsley , W. Yan , S. B. Yang , J. Yelton , J. H. Yin , Y. Yook , C. Z. Yuan , Z. P. Zhang , V. Zhilich , V. Zhukova 

APPENDIX A. SUPPLEMENTARY MATERIAL

Figure 5 is the illustration of helicity angles definitions for $\Lambda_c^+ \rightarrow \Lambda\pi^+$ decays and $\Lambda_c^+ \rightarrow \Sigma^0\pi^+$ decays. Figures 6 and 7 show the $M(\Lambda_c^+)$ distribution of the combined Λ_c^+ and $\bar{\Lambda}_c^-$ sample and the projection of the fit to extract the signal yields. Figures 8 and 9 show the fits to helicity angle distributions. The fitted slopes $k = \alpha_{\Lambda_c^+}\alpha_-$ and $\bar{k} = \alpha_{\bar{\Lambda}_c^-}\alpha_+$ are used to determine $\alpha_{\Lambda_c^+}$ and $\alpha_{\bar{\Lambda}_c^-}$ respectively, and then to calculate A_{CP}^α .

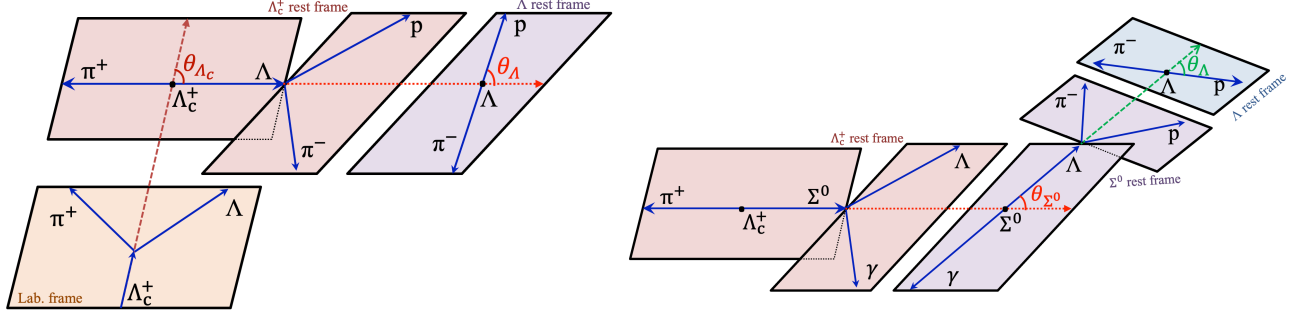


FIG. 5. Schematic plot showing the helicity angles: (left) $\theta_{\Lambda_c^+}$ and θ_{Λ} in $\Lambda_c^+ \rightarrow \Lambda\pi^+$, $\Lambda \rightarrow p\pi^-$; and (right) θ_{Σ^0} and θ_{Λ} in $\Lambda_c^+ \rightarrow \Sigma^0\pi^+$, $\Sigma^0 \rightarrow \gamma\Lambda$, $\Lambda \rightarrow p\pi^-$.

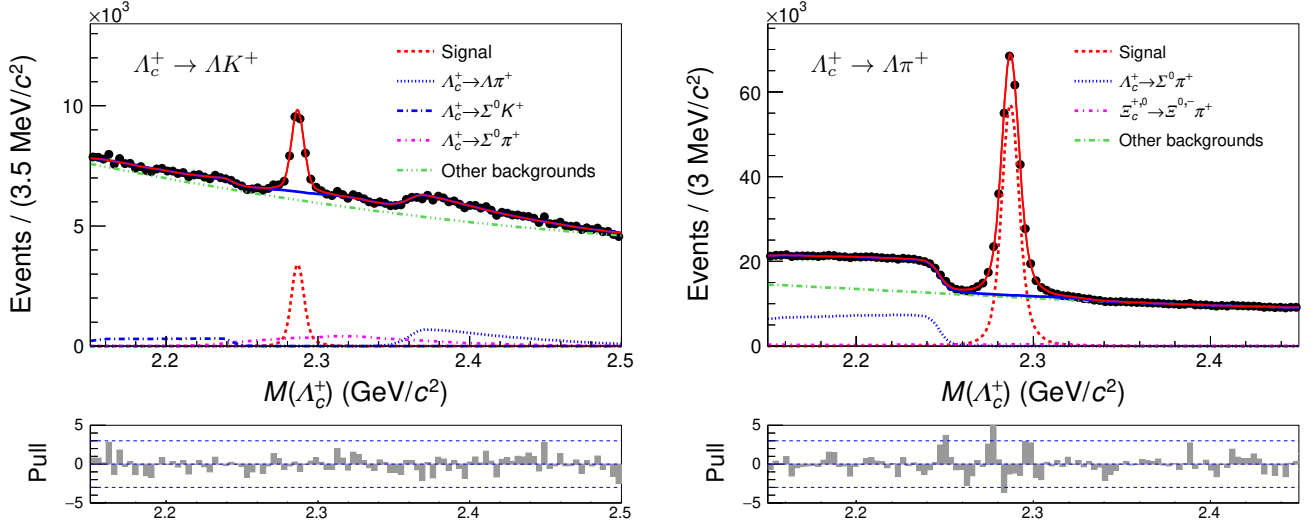


FIG. 6. The fit results of Λ_c^+ invariant mass distributions for $\Lambda_c^+ \rightarrow \Lambda K^+$ and $\Lambda_c^+ \rightarrow \Lambda\pi^+$ decays. The red curve shows the total fit result, and the blue curve the total background; the dashed curves show the components of signal and backgrounds. The fit qualities, χ^2 divided by the number of degrees of freedom, are $\chi^2/91 = 1.12$ and $\chi^2/91 = 1.38$, respectively.

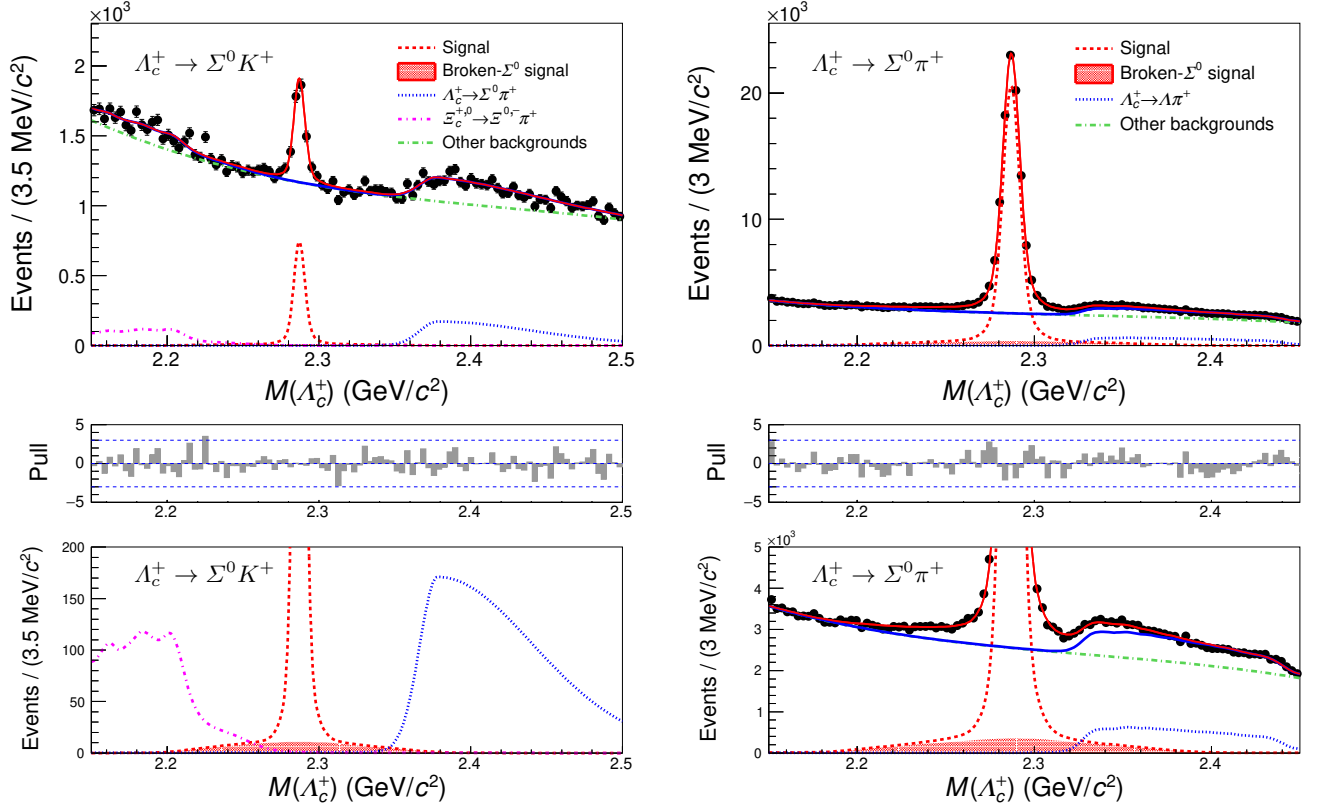


FIG. 7. The fit results of Λ_c^+ invariant mass distributions for $\Lambda_c^+ \rightarrow \Sigma^0 K^+$ and $\Lambda_c^+ \rightarrow \Sigma^0 \pi^+$ decays. The red curve shows the total fit result, and the blue curve the total background; the dashed curves show the components of signal (including the broken- Σ^0 signal) and backgrounds. The fit qualities, χ^2 divided by the number of degrees of freedom, are $\chi^2/91 = 1.38$, and $\chi^2/92 = 1.07$, respectively. The bottom figures are the enlarged view to show the distributions of broken- Σ^0 signal (red-filled histogram) and the peaking backgrounds more clearly.

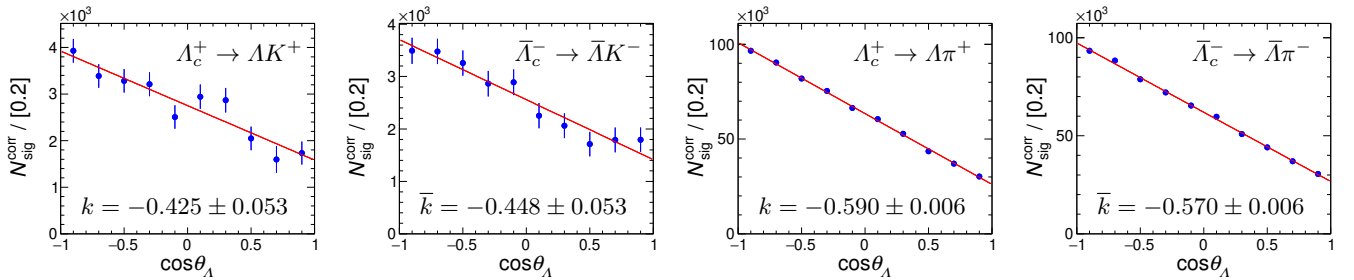


FIG. 8. The $\cos\theta_\Lambda$ distributions of $\Lambda_c^+ \rightarrow \Lambda K^+$ and $\Lambda_c^+ \rightarrow \Lambda \pi^+$ after efficiency-correction. We fit it with a linear function of $1 + \alpha_{\Lambda_c^\pm} \alpha_\mp \cos\theta_\Lambda$ with the χ^2 divided by the number of degrees of freedom, $\chi^2/9 = 1.04, 0.57, 1.25$, and 0.88 , respectively, and the fitted slope values ($k = \alpha_{\Lambda_c^+} \alpha_-$ and $\bar{k} = \alpha_{\Lambda_c^-} \alpha_+$) are shown.

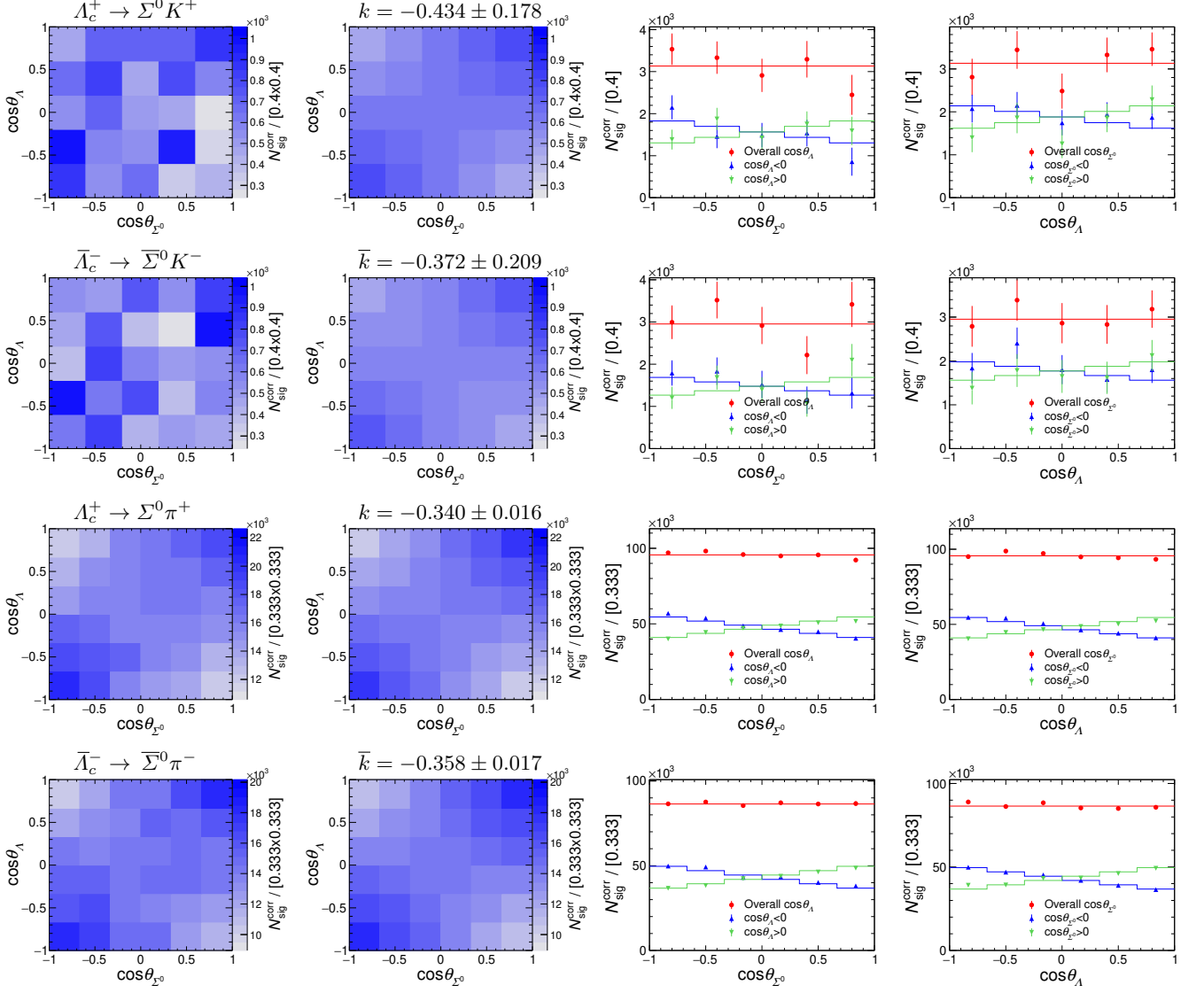


FIG. 9. The $[\cos\theta_{\Sigma^0}, \cos\theta_{\Lambda}]$ distributions of (upper plots) $\Lambda_c \rightarrow \Sigma K$ and (lower plots) $\Lambda_c \rightarrow \Sigma\pi$ decays. The first column shows the distributions after efficiency correction; the second column shows the respective fit results using a linear function $1 - \alpha_{\Lambda_c^\pm} \alpha_{\mp} \cos\theta_{\Sigma^0} \cos\theta_{\Lambda}$. Fitted slope values ($k = \alpha_{\Lambda_c^+} \alpha_{-}$ and $\bar{k} = \alpha_{\Lambda_c^-} \alpha_{+}$) are shown. The χ^2 divided by the number of degrees of freedom is $\chi^2/24 = 0.82$ and 0.78 for the ΣK fits and $\chi^2/35 = 1.35$ and 1.05 for the $\Sigma\pi$ fits. The third column shows the projections of the $\cos\theta_{\Sigma^0}$ distributions (point with error) and the fit results (histograms) in overall (red) or negative (blue) or positive (green) $\cos\theta_{\Lambda}$ region; vice versa in fourth column. The absolute slopes of all projections in slices equal half of the fitted slope listed in the second column.